Norwegian University
of Life Sciences

Master's Thesis 2017 30 ECTS
Faculty of Science and Technology

Adapting a Deep Bed Filtration Model to Real-World Data

Erlend Øydvin
Vann- og miljøteknikk

Summary

Safe and clean drinking water is a limited resource and pathogenic microorganisms might pose a threat for consumers if the water is not treated properly. Coagulation- and filtration is much used in drinking water treatment plants in Norway, but there is a need for better documentation on virus removal in these plants.

Virus removal was recently studied in a pilot scale two media contact-filtration plant at the Norwegian University of Life Sciences. The experiment measured turbidity, headloss, *E. Coli* and two types of viruses at 8 filter depths, 12 times through an 18 hour long filtration cycle. In this thesis we have derived the mathematical models that govern the removal of turbidity and virus in a rapid sand filter. We have also fitted a mathematical filtration model to the measured turbidity so that later work can solve the virus problem.

Two separate investigations were performed, one for the upper medium and one for the lower medium. In each medium, models allowing particle detachment and models that do not allow particles to detach were compared.

In the upper medium the model gave best fit to the measured data if the particles were allowed to detach from the filter grains. In the lower medium the model allowing particles to detach gave almost as good a fit to the measurements as the model that did not allow the particles to detach. This could indicate that particles detach in the upper medium and not in the lower medium.

Samandrag

Reint og trygt drikkevatn er ein begrensa ressurs i verda, og patogene mikroorganismar i drikkevatnet kan utgjere ein fare for konsumentane dersom vatnet ikkje vert behandla riktig. Koagulering- og filtrering og er ein mykje brukt renseteknikk i Noreg, men det er behov for betre dokumentasjon av virusfjerning i denne typen anlegg.

Virusfjerning vart nyleg undersøkt i eit pilotskala to-media kontaktfiltreringsanlegg i eit doktorgradsarbeid ved Norges miljø- og biovitenskapelige universitet. Forsøket målte turbiditet, trykktap, *E. Coli*, og to typar virus, på 8 ulike djup i filteret, 12 gonger under ein 18 timar lang filtreringssyklus. I denne oppgåva har me utleia dei matematiske modellane som skildrar korleis turbiditet og virus vert fjerna i eit sandfilter. Me har også og tilpassa ein matematisk filtreringsmodell til målt turbiditet, slik at seinare arbeid kan løyse virusproblemet.

Det var gjort to separate undersøkingar, ein for det øvre filtermediet og ein for det nedre filtermediet. I kvar av media vart modellar som tillet at partiklar løsnar frå filtermediet og modellar som ikkje tillet at partiklar løsnar frå filtermediet samanlikna.

For det øvre mediet gav modellen best samsvar med dei målte data når partiklane fekk lov til løsne frå filtermediet. I det nedre mediet gav modellen som tillet at partiklar løsnar nesten like godt samsvar med målte data som modellen som ikkje tillet at partiklane fekk lov til å løsne. Dette kan være ein indikasjon på at partiklar løsnar i det øvre mediet, medan dei ikkje løsnar i det nedre mediet.

Acknowledgements

This thesis is the final work of my 5-year Master's degree in environmental engineering at the Norwegian University of Life Sciences.

I want to thank my main supervisor Vegard Nilsen for coming up with the idea for this thesis, organizing the meetings and reading through the thesis. This work would definitely not be possible without you. I also want to thank my co-supervisors Bjørn Fredrik Nielsen and Lars Molstad for making it possible for me to understand some of the mathematics and physics that is going on in deep bed filtration. It has been challenging, but fun to work with you.

Ås, May, 2017

Erlend Øydvin

Table of Contents

List of Figures

List of Tables

Nomenclature

Acronyms

E. Coli	*Escherichia Coli*
DWTP	Drinking water treatment plant
L	Length
NOM	Natural organic matter
ODE	Ordinary differential equation
P1	First-order polynomail
P2	Second-order polynomail
P3	Third-order polynomail
PDE	Partial differential equation
T	Time
UV	Ultraviolet

Greek Symbols

ϵ	Volume of water per volume of filter	$[L^3/L^3]$
ϵ_0	The initial porosity of the filter bed	$[L^3/L^3]$
ϵ_d	Porosity of deposited particles	$[L^3/L^3]$
λ	The filtration function	$[1/L]$
λ_0	Initial removal efficiency	
σ	Volume of deposited particles per volume of filter	$[L^3/L^3]$
σ_v	Volume of deposited virus per volume of filter	$[L^3/L^3]$
σ_{turb}	Retained turbidity	[NTU]
σ_{ult}	Maximum volume of deposits that the filter can hold	$[L^3/L^3]$

Roman Symbols

c	Volume of particles in the water phase per volume of water	$[L^3/L^3]$
c_v	Volume of virus in the water phase per volume of water	$[L^3/L^3]$
c_{inn}	Boundary condition upper medium	$[L^3/L^3]$
c_{turb}	Turbidity in the water phase	[NTU]
c_{upper}	Boundary condition lower medium	$[L^3/L^3]$
d_g	Diameter of a filter grain	[L]
d_p	Diameter of a particle	[L]
f_1	Filtration function for the lower medium	[1/L]
f_2	Filtration function for the upper medium	[1/L]
L_g	Length of the simulated grid	[L]
t	Temporal coordinate	[T]
T_g	Stop time of the simulated grid	[T]
u	Darcy velocity of the fluid	[L/T]
z	Spatial coordinate	[L]
z_1	Coordinate for the end of the upper medium	[L]
z_2	Coordinate for the end of the lower medium	[L]

Chapter 1

Introduction

In this thesis we will examine the dynamic process inside a rapid sand filter using mathematical filtration theory. We will first look at the role of rapid sand filters in a drinking water treatment plant (DWTP) and present standard filtration theory. Then we will derive mathematical methods that we will apply on real world data in an attempt to adapt a mathematical filtration function.

1.1 Drinking water treatment

The goal of drinking water treatment is to treat raw water so that it is easy to distribute, aesthetic, have a good taste and is safe to drink – all of this within a reasonable budget. These factors are usually coupled, meaning that making the water safer to drink may, if not done optimally, come at the expense of for example budget, taste or corrosion of pipes. Since no raw water, DWTP, distribution system or operating staff is similar, finding a general treatment procedure that works under all of these conditions has not yet been achieved. However, there are some common treatment processes that can be optimized for each individual treatment plant (Eikebrokk, 2012).

1.1.1 The water treatment process

According to Folkehelseinstituttet (2016) the main components we wish to remove from the raw water are pathogenic micro-organisms, natural organic matter (NOM), color, particles, corrosive components, taste and odour and organic micropollutants. In addition we also need to remove iron, manganese, radon, hydrogen sulphide and fluoride. Large particles can be removed in a pre-treatment stage,

usually using a sieve (0,1 - 0,4 mm openings). In the next stage a chemical coagulant is typically applied. The coagulant destabilizes the particles, making them able to collide and form larger particles. By carefully stirring the water in a process called flocculation, these particles will collide and form larger particles, flocs. The flocs can be separated from the water using sedimentation or flotation. However, as sedimentation and flotation are not able to remove all flocs it is often necessary to apply filtration. Filtration can also be a part of the pre-treatment. It is important to note that by filtration we mean deep bed filtration and not membrane filtration.

In order to inactivate microbial pathogens, most DWTP apply some kind of disinfection stage. Usually this is chlorination, ozonation or ultraviolet (UV) radiation. All of these disinfection stages cause problems if applied on water with high concentrations of particles and/or NOM. The reaction between chlorine and natural organic matter produces carcinogenic by-products (Boorman et al., 1999), particles can shield the pathogens from the UV radiation (Hijnen and Medema, 2010) and ozonation has been reported to produce dangerous by-products such as bromide (Havelaar et al., 2000). Therefore most DWTPs remove particles and natural organic matter from the raw water before it is disinfected.

1.1.2 Rapid sand filtration

Rapid sand filtration has been applied in DWTPs since the early 20th century. Originally its main purpose was to remove particles, but it can be designed to remove NOM as well (Crozes et al., 1995). When NOM removal is the main goal, the process typically involves higher coagulation doses and stricter regulation of pH and is often referred to as enhanced coagulation (Edzwald and Tobiason, 1999).

In order to be effective, rapid sand filtration has to be preceded by a coagulation stage. This process destabilizes the particles, making it easier for them to attach to the filter grains (Bache and Gregory, 2010; O'Melia, 1985). Commonly used coagulants are salts of iron and aluminum. There are many mechanisms involved when a coagulant destabilizes particles. Mainly we divide them into four groups; adsorption, sweep coagulation, compression of the electric double layer and bridging (Amirtharajah and Mills, 1982). In a coagulation process all of these effects are present, although effects of adsorption is considered more important in Norwegian DWTPs.

Rapid sand filtration works by letting water flow down through a sand filter. Particles in the water will attach to the sand grains and thus be removed. There are three different configurations of a rapid sand filter, conventional, direct and contact filtration. In conventional filtration a flocculation step and a sedimentation step precede the filtration step. This configuration is usually applied for raw waters with high particle concentrations, such as water from rivers. If the water has lower concentrations of particles, direct filtration or contact filtration can be applied. In

direct filtration the filter is preceded by a flocculation stage. In contact filtration the flocculation occurs inside the filter pores (Adin and Rajagopalan, 1989).

In a typical sand filter the water enters on top of the filter and flows down through either two or three different layers of filter medium. The upper medium usually has coarser grains with low mass density whereas the lower medium has finer grains with higher mass density. The filter has a mechanism for cleaning, usually by applying a combination of air and water with higher velocity in the up-flow direction. This process is called backwashing. Due to the different mass densities in the different medium, they will remain separated after backwashing, keeping the filter's structure. The overall performance of the sand filter can be monitored by looking at the "turbidity" in the effluent. Turbidity is a measure of how much light that is reflected 90 degrees from a light beam. Many particles in the water causes more light to be reflected. When the turbidity becomes too high, the removal capacity of the sand filter has been exhausted and the filter needs to be backwashed. It is also possible to monitor the pressure required for pushing water trough the filter, known as head loss. If the head loss is too high, the filter is backwashed. In practice most DWTP backwash based on previous experience, before the turbidity rises.

A sand filter is usually backwashed about one to three times per day. One filtration cycle consists of two main stages. Initially, after a backwash, the particles will deposit on filter grains that are clean . This is called the "initial stage". The rest of the filtration cycle is called the "transient stage". The transient stage can be divided into three smaller stages. Depending on the chemical conditions of the water and the filter medium, the filter will start to capture particles. This is called the "ripening stage". The filter has poor performance and the effluent water is not distributed to consumers, but is directed to waste. After some time the filter removal becomes stable and the effluent water can be distributed. This is called the "working stage". After some more time the filter media cannot hold more particles. This causes the effluent turbidity to rise and is called the "breakthrough stage". After the breakthrough, the filter is backwashed and the cycle starts over again (Jegatheesan and Vigneswaran, 2005).

According to Adin and Rebhun (1974), at any given time, only a small portion of the filter bed takes part in the removal of particles. This suggests that the process can be though of as a ripening and breakthrough front propagating through the filter media. When the front reaches the end of the filter, the turbidity rises. Studies have shown that there is a difference in the time to breakthrough between small and large particles (Clark et al., 1992). This indicates that there are several ripening and breakthrough fronts propagating through the filter media (Moran et al., 1993).

Norwegian regulations require at last two hygienic barriers in drinking water treatment (Mattilsynet, 2011). Rapid sand filtration can, as a result of being able to remove particles, also remove many microbial pathogens (Hijnen and Medema, 2010). Thus rapid sand filtration has been considered a hygienic barrier. Since tur-

Parameter	Filtralite	Rådasand
Layer depth (m)	0.79	0.5
Grain size, nom. range (mm)	0.8-1.6	0.4-0.8
Effective grain size, d_{10} (mm)	0.95	0.4
Column diameter/d_{10} (-)	105	250
Uniformity coefficient d_{60}/d_{10} (-)	< 1.5	< 1.8
Primary porosity (-)	0.58	0.45
Bulk porosity (-)	0.80	0.45
Grain density (kg/m^3)	1260	2600
Bulk density (kg/m^3)	530	1440

Table 1.1: Data on filter materials (Nilsen, 2016).

bidity is correlated with the particle concentration (Clark et al., 1992), it has been used as an indicator for the hygienic performance of the filter. However, Petterson and Ashbolt (2016) pointed out a knowledge gap in the relation between turbidity and virus removal, revealing that turbidity might be a poor indicator for virus removal performance. This claim is supported by Eikebrokk (2012), who concluded that more data was needed on virus removal during contact filtration and direct filtration.

1.2 Pilot-scale filtration experiment

In order to examine the relation between turbidity and virus removal, a pilot-scale filtration experiment was designed by Vegard Nilsen at Norwegian University of Life Sciences (NMBU) (Nilsen, 2016). The experiment used water from the Glomma river in order to have the same working conditions as found in most Norwegian drinking water treatment plants. A transparent PVC cylinder with 10 cm diameter was filled with two types of filter medium and a support layer at the bottom. A schematic overview is presented in Figure 1.1. Figure 1.2 shows a picture of the pilot plant. The upper medium used Filtralite as filter material and the lower medium used Rådasand as filter material. The specifications of the filter materials can be found in Table 1.1. The plant was equipped with systems for control, monitoring, sampling and dosing of coagulant microorganisms. An online turbidity sensor was installed on the inlet pipe in $T1$ and another sensor was installed in $T2$, downstream of the filter. Thus the turbidity was measured continuously before and after the filter throughout the filter cycle. The filtration rate was kept constant using a feed pump. The coagulant used was PAX-18 (Kemira AS) and the pH was adjusted using hydrochloric acid. The optimal dosing was found by testing in the plant itself. In addition to manual sampling ports, ports for automatic sampling (A-H) were installed. The automatic sampler could take 8 separate channels, and store up to 12 sets of samples, corresponding to 96 samples in total. From these samples,

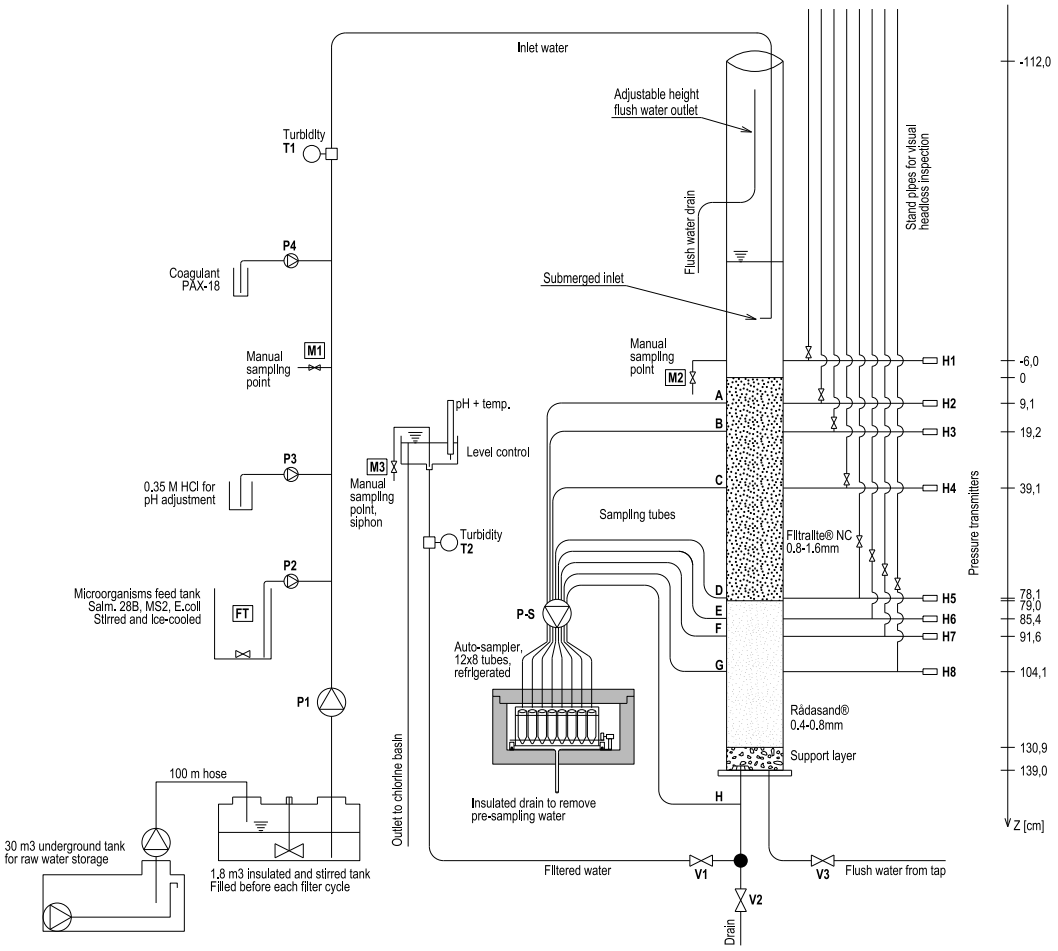

Figure 1.1: Schematic overview of the pilot plant (Nilsen, 2016).

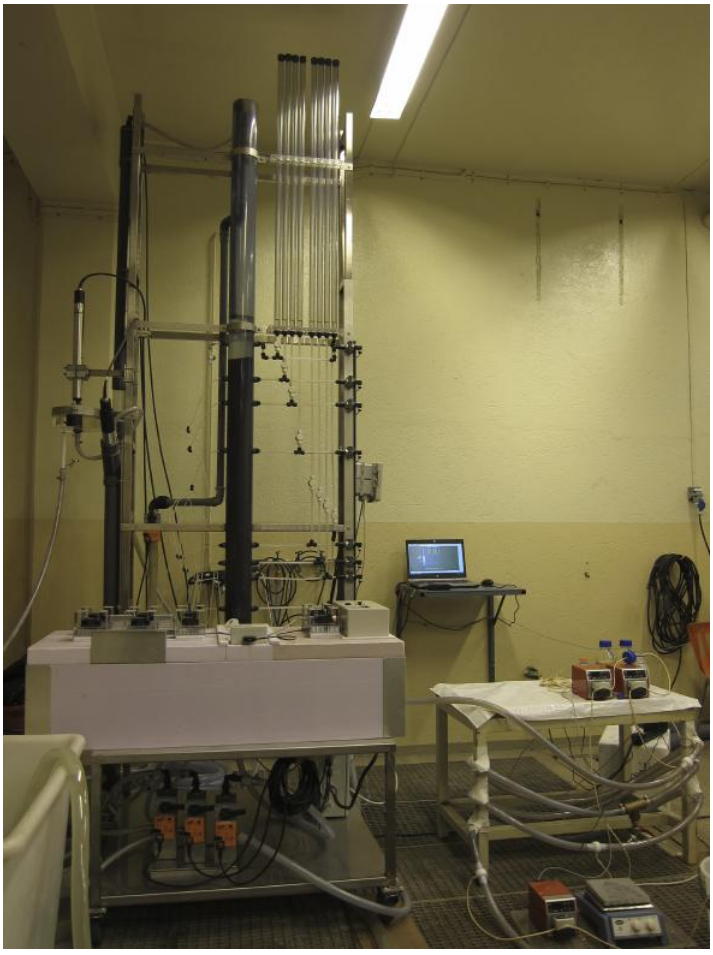

Figure 1.2: The pilot plant (Nilsen, 2016).

Parameter	Value
Raw water turbidity (NTU)	0.7-0.8
Raw water color (mg Pt/l)	26
Raw water TOC (mg/l)	3.03 ± 0.61
Raw water UV absorption (1/m)	13.1
Layer	0.5
Raw water SUVA (l/(m mg))	> 4.3
Raw water pH (-)	7.3
Raw water alkalinity (mM)	0.28
Raw water temp (°C)	15-16
Filtration rate (m/h)	5.9
Flow rate (l/min)	0.5
PAX-18 dose (mg Al/l)	1.5
HCl dose (mM)	0.12
Initial total headloss (cm)	26
s	

Table 1.2: Raw water characteristics and operation conditions (Nilsen, 2016).

turbidity, *E. coli* and two types of viruses was measured throughout an 18 hours long filtration cycle. The experiment was terminated when the turbidity reached approximately 0,3 NTU in the outlet. These 96 samples should thus capture what is normally regarded as a full filtration cycle. The measured turbidity was printed in Figure 1.3

1.3 Filtration mechanisms and models

According to Herzig et al. (1970), the flow of a suspension through a porous medium is a very complex process, due to the variety of mechanisms involved. Commonly, we divide them into two categories, mechanical filtration , where particles are retained due to effects from sieving and physiochemical filtration, where particles are retained due to physical and chemical effects. As a thumb rule mechanical filtration plays a role if $(d_p/d_g > 0,05)$, where d_p is the diameter of a particle [L], and d_g is the diameter of a filter grain [L]. In deep bed filtration the particles we wish to remove are smaller than the pores of the filter media. Thus if particles just followed the streamlines the majority of the particles would not be captured by the filter. Therefore there must exist transport mechanisms that transport particles across streamlines, attachment mechanisms that attach particles to the filter medium and (possibly) detachment mechanisms that detach particles from the filter medium (Jegatheesan and Vigneswaran, 2005). A complete filtration model should be able to predict the initial removal efficiency of a clean bed without captured particles, describe how already captured particles influence the removal efficiency

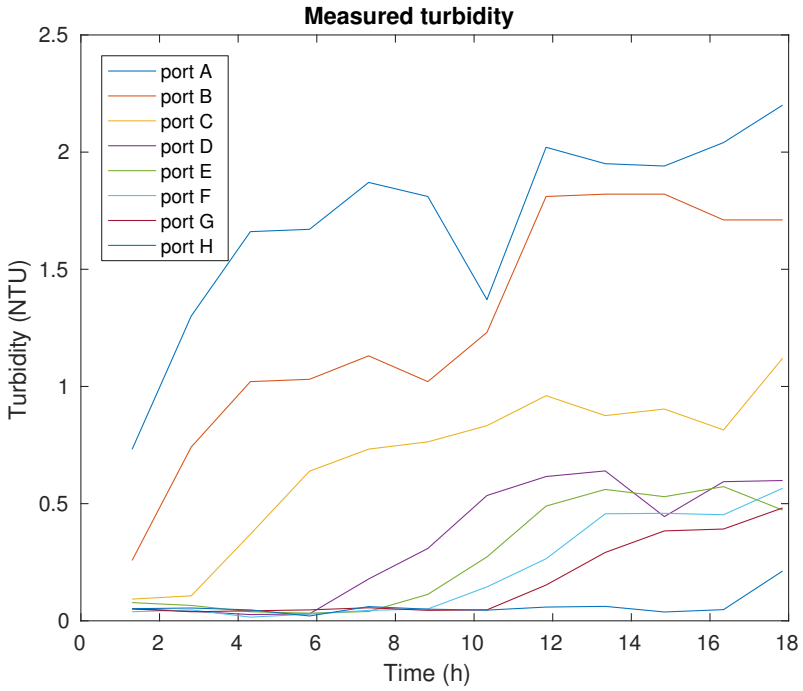

Figure 1.3: Turbidity measured in the installed ports in the filter media. See Figure 2.3.

and how they influence the flow through the medium (Nilsen, 2016). There are two main approaches to this problem, the fundamental microscopic approach and the phenomenological macroscopic approach.

1.3.1 Fundamental microscopic problem

In fundamental microscopic filtration theory we try to predict the initial removal efficiency of a clean filter bed based on first-principle models. The idea is to make mathematical descriptions of transport, attachment and detachment mechanisms and try to predict an initial removal efficiency for the filter media. However, so far these models only work well in well-controlled idealized settings (Tien and Ramaro, 2007).

1.3.2 Phenomenological macroscopic problem

In phenomenological macroscopic filtration theory we try to predict the dynamic removal efficiency for the entire filter cycle. A common approach is to perform experiments and then try to fit some mathematical model to the observations, hopefully uncovering parameters or relationships that can be generalized to more than one filter run or other experimental settings. According to Logan (2001) the rapid sand filtration model is often assumed to be advection-dominated and one dimensional. The following equation governing the particle-volume balance was derived in Appendix A

$$\frac{\partial}{\partial t}\left(\sigma + \epsilon c\right) + u\frac{\partial c}{\partial z} = 0, \tag{1.1}$$

where σ is the retention, or the volume of deposited particles per volume of filter $[\mathrm{L}^3/\mathrm{L}^3]$, ϵ is the porosity given as volume of water per volume of filter $[\mathrm{L}^3/\mathrm{L}^3]$, c is the volume of particles in the water phase per volume of water $[\mathrm{L}^3/\mathrm{L}^3]$ and u is the Darcy velocity of the fluid [L/T]. z and t are the spatial [L] and temporal [T] coordinates respectively. This equation remains the starting point for many analyses (Horner et al., 1986; Tien and Ramaro, 2007; Herzig et al., 1970; Adin and Rebhun, 1977; Alvarez, 2005).

In this thesis we are not going to find the filtration rate for viruses, but we will briefly present the governing equations. Assuming the volume the viruses take up is negligible compared to the volume of the particles, the following equation governing the virus-volume balance can be derived in the exact same way as the particle-volume balance derived in Appendix A

$$\frac{\partial}{\partial t}\left(\sigma_v + \epsilon c_v\right) + u\frac{\partial c_v}{\partial z} = 0. \tag{1.2}$$

Where σ_v is the virus retention, that is, volume of deposited viruses per volume of filter $[L^3/L^3]$ and c_v is the volume of viruses in the water phase per volume water $[L^3/L^3]$. The temporal derivative of σ and σ_v in equation (1.1) and equation (1.2) is called the filtration rate and describes the rate at which particles and virus are removed (locally) from the suspension. An expression for the filtration rate is needed in order to close the system, and there are many suggestions for the form of the filtration rate expression, or the so called filtration function. Mainly they differ as to whether particles are allowed to detach after they have attached. The first study investigating the filtration rate was done by Iwasaki (1937). He discovered through experiments that the particle concentration in the filter bed often follows an exponential distribution throughout the filter media

$$\frac{\partial c}{\partial z} = -\lambda c(z,t).$$

Where λ is known as the filter coefficients (when it is treated as a constant) and has to be determined through experiments. The main influence on the filter efficiency is the retained particles σ. Thus the filtration function is often taken as a function of the retained particles $\lambda(\sigma)$ (Tien and Ramaro, 2007). Assuming that no particles detach, the filtration rate for particles and virus was derived in Appendix B

$$\frac{\partial \sigma}{\partial t} = u\lambda(\sigma)c. \tag{1.3}$$

$$\frac{\partial \sigma_v}{\partial t} = u\lambda(\sigma)c_v. \tag{1.4}$$

From observations λ is expected to go through a ripening stage, working stage and a breakthrough stage. Thus we expect it to have the same qualitative shape as the function plotted in Figure 1.4 (Jegatheesan and Vigneswaran, 2005). There are many proposed parametric forms of $\lambda(\sigma)$. The following equation was proposed by Ives (1969) and is considered very general if particle detachment is negligible

$$\lambda(\sigma) = \lambda_0 \left(1 + \frac{\beta\sigma}{\epsilon_0}\right)^{n_1} \left(1 - \frac{\sigma}{\epsilon_0}\right)^{n_2} \left(1 - \frac{\sigma}{\sigma_{\text{ult}}}\right)^{n_3}, \tag{1.5}$$

where ϵ_0, σ_{ult}, λ_0, β, n_1, n_2 and n_3 are parameters that can be tuned to fit experimental data. ϵ_0 is the initial porosity of the filter medium given as volume of water per volume filter $[L^3/L^3]$ and σ_{ult} is the maximum volume of deposited particles per filter volume that the filter can hold $[L^3/L^3]$ and λ_0 is the initial removal efficiency of the filter medium. It must be noted that σ_{ult} cannot be larger than ϵ_0 as the filter stops filtering before it is full. Whether to include or not to include detachment was long debated Ives (1969) and Mints (1966). Today's view is that detachment do play a role, especially in the later stages of the filtration cycle (Moran et al., 1993) or during hydraulic shock loads (Kim and Lawler, 2006). In order to allow particle detachment in our model Herzig et al. (1970) have suggested the following

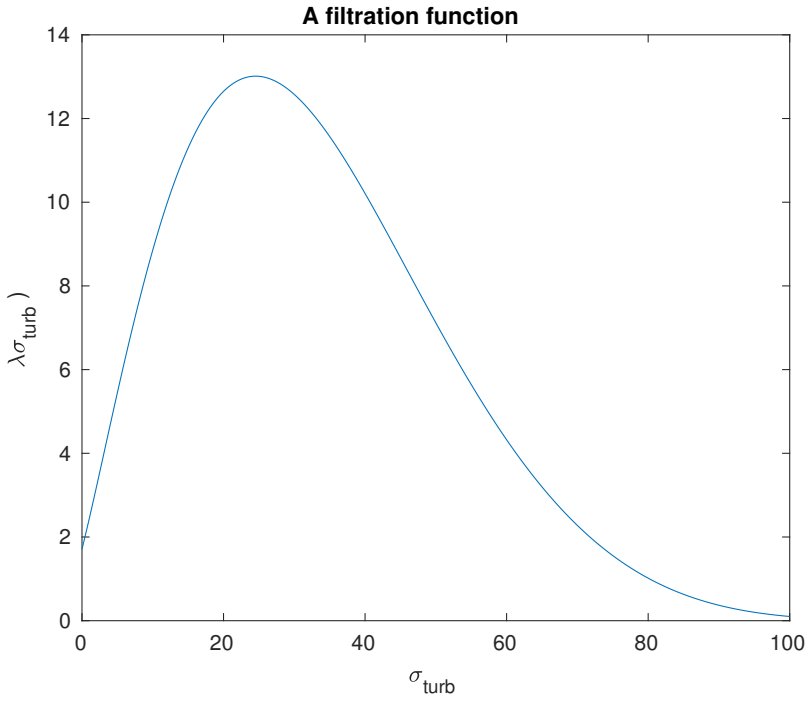

Figure 1.4: The proposed qualitative shape of the filtration function.

filtration function

$$\frac{\partial \sigma}{\partial t} = u\lambda(\sigma)c + b_1\sigma. \tag{1.6}$$

Here u, $\lambda(\sigma)$ and c are the same as in equation (1.3) and b_1 is a parameter that needs to be estimated. For convenience we define two general filtration functions for particles and for virus respectively

$$\frac{\partial \sigma}{\partial t} = f\left(u, c, \sigma\right), \tag{1.7}$$

$$\frac{\partial \sigma_v}{\partial t} = f_v\left(u, c_v, \sigma\right). \tag{1.8}$$

Equation (1.5) can be compared with simpler filtration functions in order to test whether introducing the six fitting parameters makes any sense. In this thesis we will compare equation (1.5) with a first-order polynomial (P1), a second-order

polynomial (P2) and a third-order polynomail (P3)

$$\lambda(\sigma) = a_0 + a_1\sigma, \tag{1.9}$$

$$\lambda(\sigma) = a_0 + a_1\sigma + a_2\sigma^2, \tag{1.10}$$

$$\lambda(\sigma) = a_0 + a_1\sigma + a_2\sigma^2 + a_3\sigma^3. \tag{1.11}$$

Where a_0, a_1, a_2 and a_3 are parameters that must be determined through fitting to data.

1.4 Problem statement

The ultimate goal of the experiment described in section 1.2 is to explain how virus removal is related to particle removal using mathematical filtration theory. This thesis will focus on finding a model that can describe the particle removal, so that later work can continue with the virus removal problem.

In order to do so we will reformulate and simplify the mathematical equations introduced above that govern the filtration cycle. These reformulations have been published before (Herzig et al., 1970; Tien and Ramaro, 2007), but the derivations were not easy to follow. This thesis will therefore emphasis transparency using well-known mathematical techniques in the derivations.

The derived equations will be used to explore models with filtration rates given as equation (1.7) with filtration functions given by equation (1.5), equation (1.9), equation (1.10) and equation (1.11) fit the turbidity measured in the experiment described in Section 1.2. An important aspect of this investigation will be to determine whether the particles must be allowed to detach in order to fit the data.

Chapter 2

Methods

2.1 Solving the forward problem

We wish to fit a particle-volume filtration model to the observed data. This requires solving the volume balance equation (1.1) with a filtration rate given as equation (1.7). Assuming that the the filter media is initially clean, for a given set of parameters the full closed system for particle-volume consentrations in the upper medium can be written as

$$\frac{\partial}{\partial t}(\sigma + \epsilon c) + u\frac{\partial c}{\partial z} = 0, \tag{1.1}$$

$$\frac{\partial \sigma}{\partial t} = f_1(u, c, \sigma), \tag{1.7}$$

$$c(0, t) = c_{\text{inn}}, \tag{2.1}$$

$$c(z, 0) = \sigma(z, 0) = 0, \tag{2.2}$$

where $z \in [0, z_1]$, z_1 is the coordinate for the end of the upper medium [L], c_{inn} is the particle-volume consentration of particles going in to the upper filter medium [L^3/L^3] and f_1 is the filtration function for the upper medium [1/L]. The output from the upper medium becomes input for the lower medium, hence

$$\frac{\partial}{\partial t}(\sigma + \epsilon c) + u\frac{\partial c}{\partial z} = 0, \tag{1.1}$$

$$\frac{\partial \sigma}{\partial t} = f_2(u, c, \sigma), \tag{1.7}$$

$$c(z_1, t) = c_{\text{upper}}, \tag{2.3}$$

$$c(z, 0) = \sigma(z, 0) = 0, \tag{2.4}$$

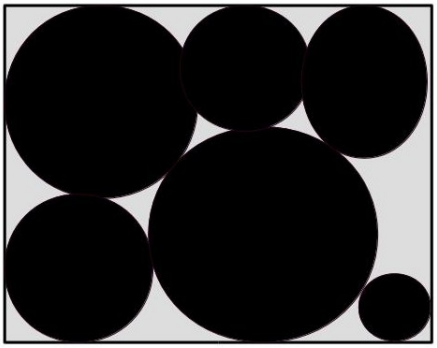

Figure 2.1: Particles (black) generally take up more volume when strained since they also occupy the volume in between them (grey).

where $z \in [z_1, z_2]$, z_2 is the coordinate for the end of the lower medium [L], c_{upper} is the particle-volume consentration of particles going out of the upper filter medium [L^3/L^3] and f_2 is the filtration function for the lower medium [1/L]. Solving this system produces an output in the form of particle-volume concentrations and is often called the "forward problem". Finding parameters that make the model consistent with observations requires us to solve the forward problem many times with different parameters. The parameters that best describe the observations is called an optimum. This problem is called the "inverse problem". In order to solve the inverse problem we need to develop a fast and reliable way of solving the forward problem.

Solving equation (1.1) and equation (1.7) in their current form is hard and not very efficient. According to Herzig et al. (1970) a common simplification is to assume a constant porosity throughout the filter cycle. This assumption greatly simplifies the forward problem. In this thesis we will mainly assume constant porosity, but we will also present a more general derivation of the solution to the system where the porosity may be allowed to change, see Appendix D. Now we will briefly discuss what assumptions we are making when assuming constant porosity. According to Figure 2.1, particles captured in a filter occupy more volume than they would in the free water phase. Thus the porosity is a function of the captured particles and how much volume the captured particles occupy. According to Herzig et al. (1970) we can express the porosity as

$$\epsilon = \epsilon_0 - \frac{\sigma}{1 - \epsilon_d}. \tag{2.5}$$

Where ϵ_d is the porosity of the deposits [L^3/L^3] and ϵ_0 is the initial porosity [L^3/L^3].

Inserting equation (2.5) into equation (1.1) we get

$$\frac{\partial}{\partial t}\left(\sigma + \epsilon_0 c - \frac{\sigma}{1-\epsilon_d}c\right) + u\frac{\partial c}{\partial z} = 0.$$

By the product rule

$$\frac{\partial \sigma}{\partial t} + \epsilon_0 \frac{\partial c}{\partial t} - \frac{1}{1-\epsilon_d}\left(\sigma\frac{\partial c}{\partial t} + c\frac{\partial \sigma}{\partial t}\right) + u\frac{\partial c}{\partial z} = 0.$$

For situations where the concentrations are low, this can be simplified to

$$\epsilon_0 \frac{\partial c}{\partial t} + u\frac{\partial c}{\partial z} = -\frac{\partial \sigma}{\partial t}. \tag{2.6}$$

According to Herzig et al. (1970) this is always true for deep filtration where concentrations are low.

2.1.1 Upwind scheme

The simplest way of solving equations on the form of equation (2.6) is applying a finite difference method called upwind scheme (LeVeque, 1992; Richard E. Ewing, 2001). Inserting the general filtration function described by equation (1.7) into the conservation equation (2.6) we get

$$\epsilon_0 \frac{\partial c}{\partial t} + u\frac{\partial c}{\partial z} = -f(u, c, \sigma). \tag{2.7}$$

Rearranging

$$\frac{\partial c}{\partial t} + \frac{u}{\epsilon_0}\frac{\partial c}{\partial z} = -\frac{1}{\epsilon_0} f(u, c, \sigma). \tag{2.8}$$

We wish to sequentially solve for $c(z,t)$ and $\sigma(z,t)$ with the two independent variables z and t on the intervals $0 \leq z \leq L_g$ and $0 \leq t \leq T_g$. We proceed by dividing the intervals into equally long subintervals, producing a grid over the region in which we will attempt to approximate a solution. We define the step-length in the z direction to be $h = z_j - z_{j-1}$ and the step-length in the t direction to be $k = t_n - t_{n-1}$, thus h and k could then be written as

$$h = \frac{L_g}{J}, \qquad k = \frac{T_g}{N}.$$

where J is the total number of intervals along the z-axis, L_g is the length of the filter medium, N is the number of intervals along the t-axis and T_g is the stopping time. By discretizing the derivatives in equation (2.8) and equation (1.7) using forward Euler differences for the temporal derivatives and backward Euler differences for

the spatial derivatives we get

$$\frac{\partial c}{\partial t}(z_j, t_n) \approx \frac{c_{j,n+1} - c_{j,n}}{k}, \tag{2.9}$$

$$\frac{\partial c}{\partial z}(z_j, t_n) \approx \frac{c_{j,n} - c_{j-1,n}}{h}, \tag{2.10}$$

$$\frac{\partial \sigma}{\partial t}(z_j, t_n) \approx \frac{\sigma_{j,n+1} - \sigma_{j,n}}{k}. \tag{2.11}$$

Inserting these results into equation (2.8) and equation (1.7) and rearranging

$$c_{j,n+1} = -\frac{k}{h}\frac{u}{\epsilon_0}(c_{j,n} - c_{j-1,n}) + c_{j,n} - \frac{k}{\epsilon_0} f(u_{j,n}, c_{j,n}, \sigma_{j,n}), \tag{2.12}$$

$$\sigma_{j,n+1} = k f(u_{j,n}, c_{j,n}, \sigma_{j,n}) + c_{j,n}. \tag{2.13}$$

Although suffereing from numerical diffusion (Richard E. Ewing, 2001), this scheme will generate a stable solution if

$$\frac{ku}{h\epsilon_0} < 1, \quad u > 0, \tag{2.14}$$

given boundary conditions by equation (2.1) or equation (2.3) and initial condition by equation (2.2). We will use the upwind scheme for comparisons with other schemes.

2.1.2 Method of characteristics

It is common to simplify equation (2.6) by dropping the temporal derivative of c. This has been done by Iwasaki (1937) and is the same as Tien and Ramaro (2007) and Herzig et al. (1970) refers to as a formulation with a "corrected time". We found the concept of corrected time to be a little vague, therefore we will use the method of characteristics to arrive at the same results. Rearranging equation (2.6) we get

$$\frac{\epsilon_0}{u}\frac{\partial c}{\partial t} + \frac{\partial c}{\partial t} = -\frac{1}{u}\frac{\partial \sigma}{\partial t}. \tag{2.15}$$

By the multivariate chain rule

$$\frac{dc}{ds} = \frac{\partial c}{\partial t}\frac{dt}{ds} + \frac{\partial c}{\partial z}\frac{dz}{ds}. \tag{2.16}$$

Equation (2.15) has the same form as equation (2.16) if we let

$$\frac{dt}{ds} = \frac{\epsilon_0}{u}, \tag{2.17}$$

$$\frac{dz}{ds} = 1, \tag{2.18}$$

$$\frac{dc}{ds} = -\frac{1}{u}\frac{\partial \sigma}{\partial t}. \tag{2.19}$$

Noticing that u and ϵ_0 were held constant we integrate equation (2.17) and equation (2.18) along s

$$t(s) = \frac{\epsilon_0}{u}s + t_0, \tag{2.20}$$

$$z(s) = s + z_0. \tag{2.21}$$

Equation (2.20) and equation (2.21) are called the characteristic lines of equation (2.15) and is illustrated in Figure 2.2. Rearranging equation (2.19) we get

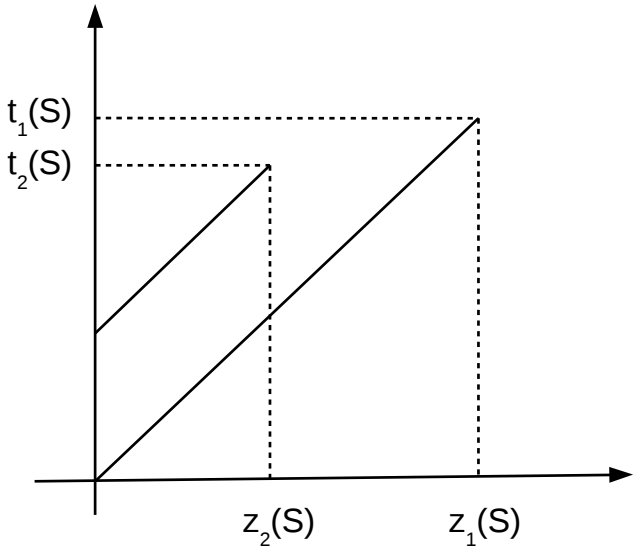

Figure 2.2: The characteristic lines of equation (2.6)

$$\frac{\partial \sigma}{\partial t} + u\frac{dc}{ds} = 0. \tag{2.22}$$

According to Horner et al. (1986) this can be thought of as following a particle along its path through the filter medium. We note that for small s, small ϵ_0 and large u, following the characteristic line defined by equation (2.20) and equation (2.21) is approximately the same as following the t-axis. Using this approximation we can simplify equation (2.22) into

$$\frac{\partial \sigma}{\partial t} + u\frac{dc}{dz} = 0. \tag{2.23}$$

This is equivalent to what Herzig et al. (1970) refers to as the "3rd approximation". Equation (2.23) and equation (1.7) can be solved sequentially using a simple forward Euler scheme. Inserting equation (1.7) into equation (2.22) we get

$$\frac{dc}{ds} = -\frac{1}{u}f(u, c, \sigma)., \tag{2.24}$$

We wish to sequentially solve for $c(z,t)$ and $\sigma(z,t)$ along the z-axis and t-axis on the interval $0 \leq z \leq L_g$ and $0 \leq t \leq T_g$. We proceed by dividing the intervals into equally long subintervals, producing a grid over the region in which we will attempt to approximate a solution. We define the step-length along the z-axis to be $h = h_j - h_{j-1}$ and the step-length along the t-axis to be $k = t_n - t_{n-1}$, thus h and k could then be written as

$$h = \frac{L_g}{J}, \qquad k = \frac{T_g}{N}.$$

where J is the total number of intervals along the z-axis, L_g is the length of the filter medium, N is the number of intervals along the t-axis and T_g is called stopping time. By discretizing the derivatives in (1.7) and (2.22) using forward Euler we get

$$\frac{\partial c}{\partial z}(z_j, t_n) \approx \frac{c_{j+1,n} - c_{j,n}}{h},$$
$$\frac{\partial \sigma}{\partial t}(z_j, t_n) \approx \frac{\sigma_{j,n+1} - \sigma_{j,n}}{k}.$$

By inserting these results into equation (1.7) and equation (2.22) and rearranging we get the following system which can be solved sequentially.

$$c_{j+1,n} \approx c_{j,n} - \frac{h}{u}f(u_{j,n}, c_{j,n}, \sigma_{j,n}), \tag{2.25}$$
$$\sigma_{j,n+1} \approx \sigma_{j,n} + kf(u_{j,n}, c_{j,n}, \sigma_{j,n}). \tag{2.26}$$

With boundary conditions given by equation (2.1) or equation (2.3) and initial condition given by equation (2.2) this scheme will converge towards the exact solution for a fine spaced grid. However, it might be hard to know how fine the grid needs to be. The scheme would also require quite a lot of computations, which is not good when we need to solve our system many times. A good thing about this scheme is

that it is able to handle many forms of $f(u, c, \sigma)$.

2.1.3 Solving a system of ODEs

This method was first outlined by Herzig et al. (1970). It notices that if the filtration-function is given in a specific form, the system can be reduced to two ordinary differential equations, which in turn can be solved separately using standard software packages. We will use the method of characteristics to arrive at the same results. These results was derived by Bjørn Fredrik Nilsen. By applying the method of characteristics on equation (2.6) we get the mass balance equation (1.3) and particle conservation on the form of equation (2.23)

$$\frac{\partial \sigma}{\partial t} + u\frac{dc}{dz} = 0, \tag{2.27}$$

$$\frac{\partial \sigma}{\partial t} = u\lambda(\sigma)c. \tag{2.28}$$

Rearranging equation (2.28)

$$c = \frac{1}{u\lambda(\sigma)}\frac{\partial \sigma}{\partial t}. \tag{2.29}$$

Inserting equation (2.29) into equation (2.27)

$$\frac{\partial \sigma}{\partial t} + \frac{\partial}{\partial z}\left(\frac{1}{\lambda(\sigma)}\frac{\partial \sigma}{\partial t}\right) = 0. \tag{2.30}$$

By the product rule and the chain rule

$$\frac{\partial \sigma}{\partial t} + \frac{\partial}{\partial \sigma}\left(\frac{1}{\lambda(\sigma)}\right)\frac{\partial \sigma}{\partial z}\frac{\partial \sigma}{\partial t} + \frac{1}{\lambda(\sigma)}\frac{\partial}{\partial z}\frac{\partial \sigma}{\partial t} = 0. \tag{2.31}$$

Interchanging the order of the derivatives

$$\frac{\partial \sigma}{\partial t} + \frac{\partial}{\partial t}\left(\frac{1}{\lambda(\sigma)}\right)\frac{\partial \sigma}{\partial t}\frac{\partial \sigma}{\partial z} + \frac{1}{\lambda(\sigma)}\frac{\partial}{\partial t}\frac{\partial \sigma}{\partial z} = 0. \tag{2.32}$$

By the product rule and the chain rule

$$\frac{\partial \sigma}{\partial t} + \frac{\partial}{\partial z}\left(\frac{1}{\lambda(\sigma)}\frac{\partial \sigma}{\partial z}\right) = 0. \tag{2.33}$$

Rearranging

$$\frac{\partial}{\partial t}\left(\sigma + \frac{1}{\lambda(\sigma)}\frac{\partial \sigma}{\partial z}\right) = 0. \tag{2.34}$$

Which implies that

$$\frac{\partial \sigma}{\partial z} + \lambda(\sigma)\sigma = g. \tag{2.35}$$

Where

$$g = g(z) = \frac{\partial \sigma}{\partial z}(z, 0) + \lambda(\sigma(z, 0))\sigma(z, 0).$$

From the initial conditions we have that

$$c(z, 0) = \sigma(z, 0) = 0, \quad z \geq 0.$$

Assuming that equation (2.28) holds for $t = 0$

$$\frac{\partial \sigma}{\partial z}(z, 0) = 0 \quad z \geq 0,$$
$$\frac{\partial \sigma}{\partial t}(z, 0) = u\lambda(\sigma(z, 0))c(z, 0) = 0.$$

Hence

$$g(z) = 0.$$

Thus it follows from equation (2.35)

$$\frac{\partial \sigma}{\partial z} = -\lambda(\sigma)\sigma. \tag{2.36}$$

A more general derivation of this equation (2.36) was done in Appendix C. Now we need to find the particle concentration c in the water-phase. Since we know the value of σ this can easily be done by solving equation (2.23) along z, but we can do even better. Inserting equation (1.3) into equation (2.23) we get

$$\frac{\partial c}{\partial z} = -\lambda(\sigma)c. \tag{2.37}$$

Rearranging equation (2.36) and equation (2.37)

$$\frac{1}{\sigma}\frac{\partial \sigma}{\partial z} = -\lambda(\sigma),$$
$$\frac{1}{c}\frac{\partial c}{\partial z} = -\lambda(\sigma).$$

Noticing that these equations have the same mathematical form we proceed by integrating them along z

$$\ln \sigma = A(\sigma) + k_1,$$
$$\ln c = A(\sigma) + k_2.$$

Thus

$$\ln c = \ln \sigma + k.$$

We can determine k from the conditions at the inlet of the filter

$$\ln\left(\frac{c_{in}}{\sigma_{in}}\right) = k.$$

Thus

$$\frac{c}{c_{in}} = \frac{\sigma}{\sigma_{in}}. \tag{2.38}$$

2.2 Comparing the solution algorithms

Three different solution methods were derived, the upwind scheme, the sequential forward Euler scheme and the system of ODEs. All of these solution methods were tested with the same filtration functions and parameters. Although the upwind scheme seems to suffer from numerical diffusion, the methods seem to give results that are reasonably close to each other. This indicates that the results we get from the methods can be trusted.

2.3 Error

In order to say something about how well our model fit the measured data we need to introduce a way to measure the error. We proceed by organizing our model estimates and observations into two vectors, respectively $\vec{c}$ and $\vec{m}$, such that given N observations let m_i denote the i'th observed value and c_i denote the value of the model corresponding to that observation. We can define a way of measuring the error by summing the squares

$$e_s = (c - m, c - m) = \sum_{i=1}^{N} (c_i - m_i)^2 . \tag{2.39}$$

However, this definition of error does not take into account that the turbidity can be measured more accurately for low concentrations. We can let the smaller con-

centrations play a bigger role by introducing the weighted norm M^{-1} defined as

$$|\vec{x}|_{M^{-1}} = \sqrt{(\vec{x}, M^{-1}\vec{x})}, \tag{2.40}$$

where we have used the inner product notation. This norm is only defined for positive-definite M. Further, it is more practical to study the relative errors. A relative root mean square error in the M^{-1} norm can be defined as

$$RRMSE_{M^{-1}} = \sqrt{\frac{(\vec{c}-\vec{m}, M^{-1}(\vec{c}-\vec{m}))}{(\vec{m}, M^{-1}\vec{m})}}. \tag{2.41}$$

We can weight the smallest observations by letting the weights, M, in equation (2.41) be equal to $diag(\vec{m})$

$$WRRMSE_{M^{-1}} = \sqrt{\frac{\left(\vec{c}-\vec{m}, \frac{1}{\vec{m}}(\vec{c}-\vec{m})\right)}{\left(\vec{m}, \frac{1}{\vec{m}}\vec{m}\right)}} = \sqrt{\frac{\sum_{i=1}^{N} \frac{(c_i-m_i)^2}{m_i}}{\sum_{i=1}^{N} m_i}}. \tag{2.42}$$

We can weight all observations equally by letting the weights, M, in equation (2.41) be equal to the identity matrix, I

$$RRMSE_{M^{-1}} = \sqrt{\frac{(\vec{c}-\vec{m}, \vec{c}-\vec{m})}{(\vec{m}, \vec{m})}} = \sqrt{\frac{\sum_{i=1}^{N} (c_i - m_i)^2}{\sum_{i=1}^{N} {m_i}^2}}. \tag{2.43}$$

2.4 Solving the inverse problem

Solving the inverse problem involves minimizing some objective function (Bai and Tien, 2000). Since our data seems to give more accurate measurements for smaller observations the objective function should weight the smaller observations. Let M be equal to $diag(\vec{m})$ and the M^{-1} norm be defined as in equation (2.40). The objective function becomes

$$O(\vec{p}) = |\vec{c}-\vec{m}, M^{-1}(\vec{c}-\vec{m})| = \sum_{i=1}^{N} \frac{c_i - m_i}{\sqrt{m_i}}. \tag{2.44}$$

Where O is the objective function and $\vec{p}$ contains the parameters given to the objective function as a vector. This objective function was passed to MATLABs built in function "lsqnonlin" and to an implementation of a Markov chain Monte Carlo method made by Lars Molstad. Both functions try to minimize the sum of squares.

2.5 Adjusting the model to the measured data

In the experiment there were no direct measurements of the particle concentrations in the water phase. Instead turbidity was measured, which we at best can hope is proportional to the particle concentrations in the water phase (Clark et al., 1992). Mathematically we get

$$\sigma_{\text{turb}} = \alpha\sigma, \tag{2.45}$$

$$c_{\text{turb}} = \alpha c. \tag{2.46}$$

Where c_{turb} is the turbidity in the water phase, σ_{turb} is the retained turbidity and α is a scaling factor. The value of α is unknown, but it is believed that it should not exceed 400 (Nilsen, 2016). It must be noted that α is different from raw water to raw water as the particle-size distribution affects the measured turbidity (Clark et al., 1992). The partial differential operators are linear, but the function lambda might not be linear. Therefore, inserting equation (2.46) and (2.45) into equation (2.36) we get

$$\frac{\partial\sigma_{\text{turb}}}{\partial z} = -\lambda\left(\frac{\sigma_{\text{turb}}}{\alpha}\right)\sigma_{\text{turb}}. \tag{2.47}$$

Inserting equation (2.46) and (2.45) into equation (1.6) we get

$$\frac{\partial\sigma_{\text{turb}}}{\partial t} = u\lambda(\frac{\sigma_{\text{turb}}}{\alpha})c_{\text{turb}} + b_1\sigma_{\text{turb}}. \tag{2.48}$$

Inserting equation (2.46) and (2.45) into equation (2.23) we get

$$\frac{\partial c_{\text{turb}}}{\partial t} = -u\frac{\partial c_{\text{turb}}}{\partial z}. \tag{2.49}$$

Inserting equation (2.46) and (2.45) into equation (2.38) we get

$$\frac{c_{\text{turb}}}{c_{\text{turb}_{in}}} = \frac{\sigma_{\text{turb}}}{\sigma_{\text{turb}_{in}}}. \tag{2.50}$$

Using the Ives filtration function we proceed by inserting equation (2.45) into equation (1.5)

$$\lambda(\frac{\sigma_{\text{turb}}}{\alpha}) = \lambda_0\left(1 + \frac{\beta\sigma_{\text{turb}}}{\epsilon_0\alpha}\right)^{n1}\left(1 - \frac{\sigma_{\text{turb}}}{\epsilon_0\alpha}\right)^{n2}\left(1 - \frac{\sigma_{\text{turb}}}{\sigma_{\text{ult}}\alpha}\right)^{n3}. \tag{2.51}$$

For this filtration function α has to be estimated as another free parameter. Inserting equation (2.45) into equation (1.10)

$$\lambda\left(\frac{\sigma_{\text{turb}}}{\alpha}\right) = a_0 + a_1\frac{\sigma_{\text{turb}}}{\alpha} + a_2\left(\frac{\sigma_{\text{turb}}}{\alpha}\right)^2. \tag{2.52}$$

For this filtration function α just is just baked into constants a_1 and a_2 and we get

$$\lambda(\sigma_{\text{turb}}) = a_0 + a_1\sigma_{\text{turb}} + a_2\left(\sigma_{\text{turb}}\right)^2. \tag{2.53}$$

The same can be done for all of the polynomials.

2.6 Boundary conditions

The boundary condition for the upper medium was set to the mean of the turbidity recorded in the inlet $T1$ (see Figure 1.1) as the inlet turbidity should be constant throughout the experiment. Only the 5 first turbidity values was used as the 7 other turbidity values were assumed to be influenced by flocs settling on the turbidity sensor.

For the lower medium the ideal boundary condition would be the solution from the upper medium. This would allow a continuous solution throughout the upper and the lower medium. However, as all of the solutions to the upper medium gave very poor boundary conditions for the lower medium another approach using a spline of the turbidity recorded in port D (see Figure 1.1) was used. This spline was plotted along with observations from port E, F and G in Figure 2.3. The 10th observation was removed since it was assumed to be an error in the measurements.

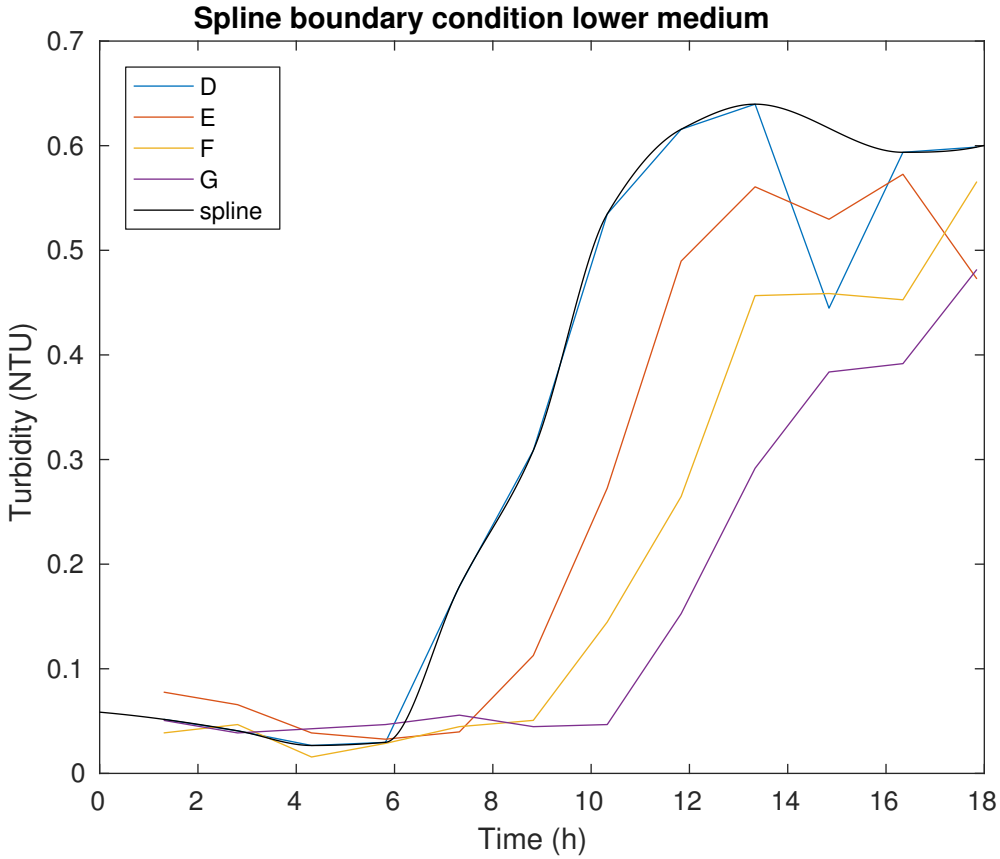

Figure 2.3: Spline following the observations in port D.

Chapter 3

Results and discussion

For all optimization runs MATLABs built in method lsqnonlin and the Markov chain Monte Carlo method gave approximately the same answers. The results shown in this section is generated by the lsqnonlin method. For all simulations the value of σ_{turb} was restricted to being positive only.

3.1 Attachment model

For models considering only attachment the ODE method using equation (2.36) and equation (2.38) were applied. This method can not take filtration functions that allow detachment, thus equation (1.3) was used for modelling the filtration rate.

3.1.1 Upper medium

For the upper medium a first-order polynomial (equation (1.9)), a second-order polynomial (equation (1.10)), a third-order polynomial (equation (1.11)), Ives' filtration function with bounded α (equation (1.5)) and Ives' filtration function with unbounded α (equation (1.5)) were considered. The optimal filtration functions $\lambda(\sigma_{\text{turb}})$ are shown in Figure 3.1. The weighted relative root mean square, as defined by equation (2.42) and the relative root mean square, as defined by equation (2.43) for the optimal filtration functions are shown in Table 3.1. The weighted relative root mean square, as defined by equation (2.42), for different choices of parameters was printed in Figure 3.2.

From Table 3.1 we can see that Ives' filtration function with bounded α has a higher error than the other functions. Even though it has 7 free parameters, it explains the data less well than the first-order polynomial, which has only 2 free parameters.

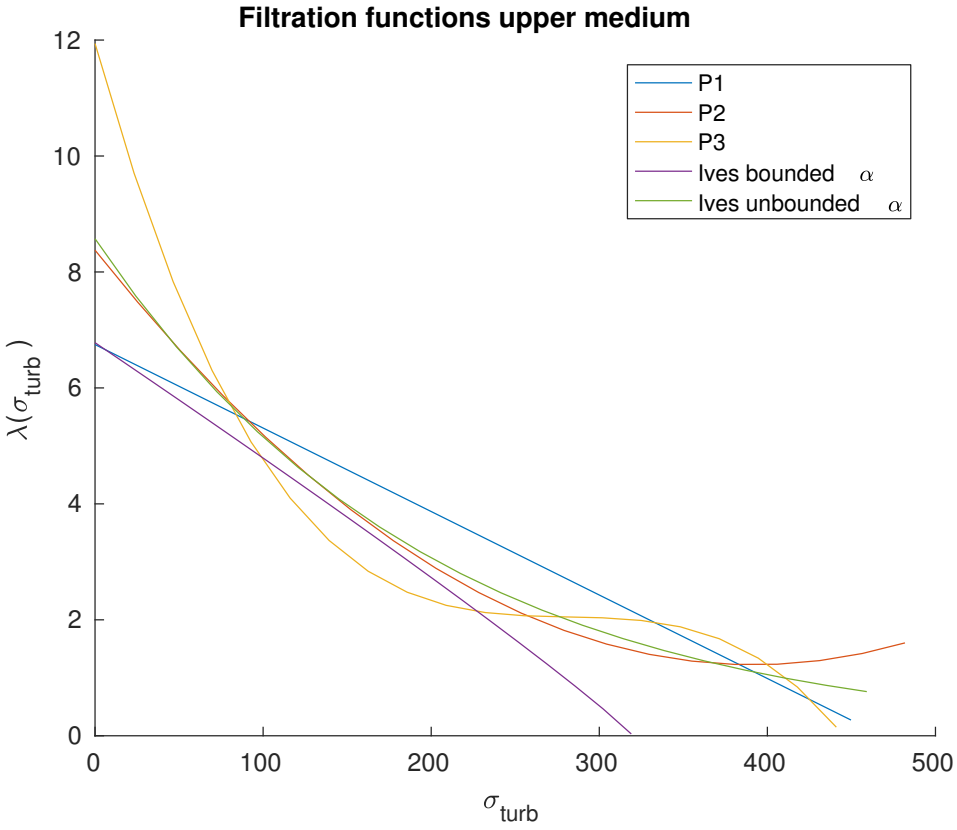

Figure 3.1: Optimal filtration functions for the upper medium considering attachment only. The upper and lower range is set by the largest and smallest σ_{turb} present in the solution.

Filtration function	Weighted RRMSE	RRMSE
P1	0.3158	0.2058
P2	0.3010	0.2057
P3	0.2932	0.2008
Ives	0.3851	0.2854
Ives unbounded α	0.3005	0.2014

Table 3.1: Weighted RRMS and RRMS for the optimal filtration functions in the upper medium considering attachment only.

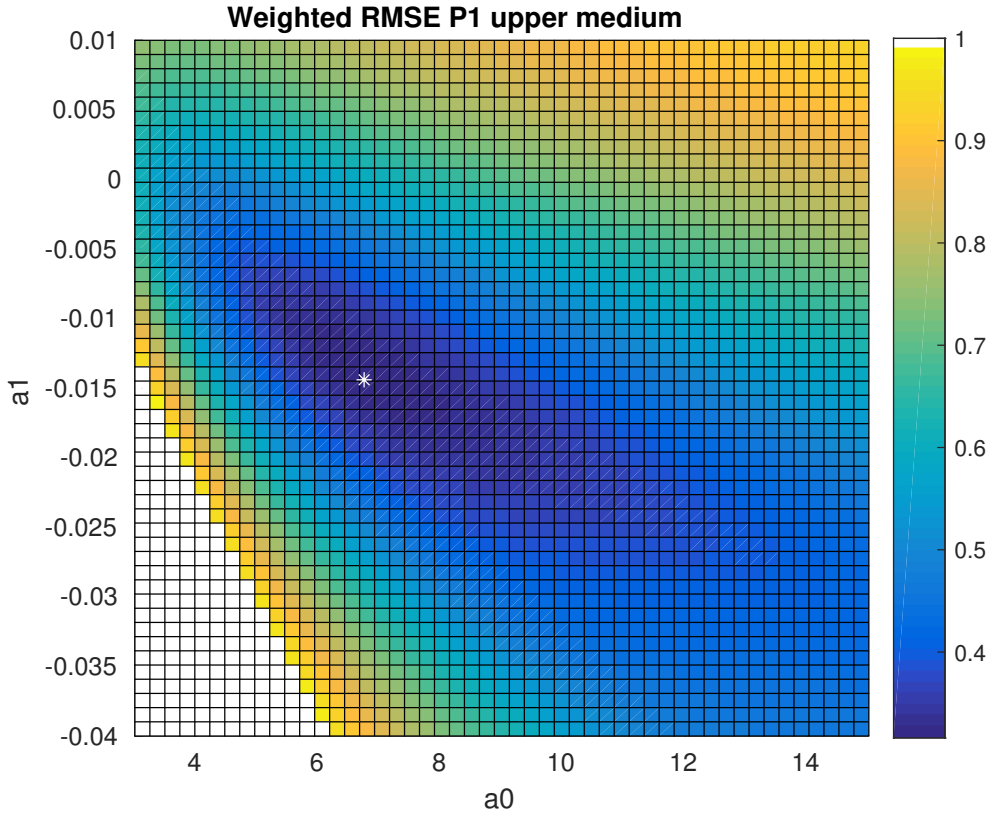

Figure 3.2: Plot of the weighted RRMS for different choices of parameters for the first-order polynomial in the upper medium considering attachment only. Dark blue colors represents parameters that give a good fit, yellow color represents parameters that give a bad fit. White cells represents parameters that gave large errors or NaN values. The white $*$ is the optimum found by the inverse solver.

	a_0	a_1	a_2	a_3			
P1	6.748	-0.014					
P2	8.376	-0.037	4.658e-05				
P3	11.940	-0.105	3.713e-4	-4.410e-7			
	λ_0	β	n_1	n_2	n_3	α	σ_{ult}
Ives	6.780	0.017	0.001	0.883	0.045	400.000	0.800
Ives_α	8.573	15.753	2.628e-07	15.969	10.842	6.648e+03	0.799

Table 3.2: The parameters for the best filtration functions in the upper medium considering attachment only. Ives_α denotes Ives filtration function with unbounded α.

Ives' filtration function with unbounded α gives a better fit. Looking at Figure 3.1 we see that Ives' filtration function with unbounded α seems to have the same qualitative shape as the second-order polynomial.

The best fit filtration functions in the upper medium are high for $\sigma_{\text{turb}} = 0$ and then decreasing with σ_{turb}. This does not fit very well with the shape one would expect for a typical filter cycle with a ripening period. However, by looking at Figure 3.3, in the first turbidity recording (approximately after 1.3 hours), we can see that the turbidity recorded in port A, B and C are already showing a rising trend, indicating that breakthrough has already occurred in these ports. In other words, the ripening part is over. Ripening can only be observed between port C and port D, and to some extent between port B and C. Since the majority of the recordings do not capture the ripening part we should not expect λ do have a ripening part either. This could explain the observed qualitative shape of the best-fit filtration functions.

The errors for the polynomials from Table 3.1 indicate that going from a first-order polynomial to a third-order polynomial does not generate a much better fit. Looking at Figure 3.2 we see that the area around the optimum is relatively flat. This could mean that there are many linear filtration functions that fit the observations sufficiently well. The first-order polynomial was used to generate a solution for the upper medium. The solution was printed in Figure 3.3

Different choices of initial values for the parameters were tested for Ives filtration function in the upper medium. This led to convergence towards different optima or just abortions due to low gradients. There were no such errors for the polynomials. This could indicate that the problem is ill-posed for the Ives filtration function, probably because it has too many parameters.

The parameters for for the best fit filtration functions in the upper medium are shown in Table 3.2.

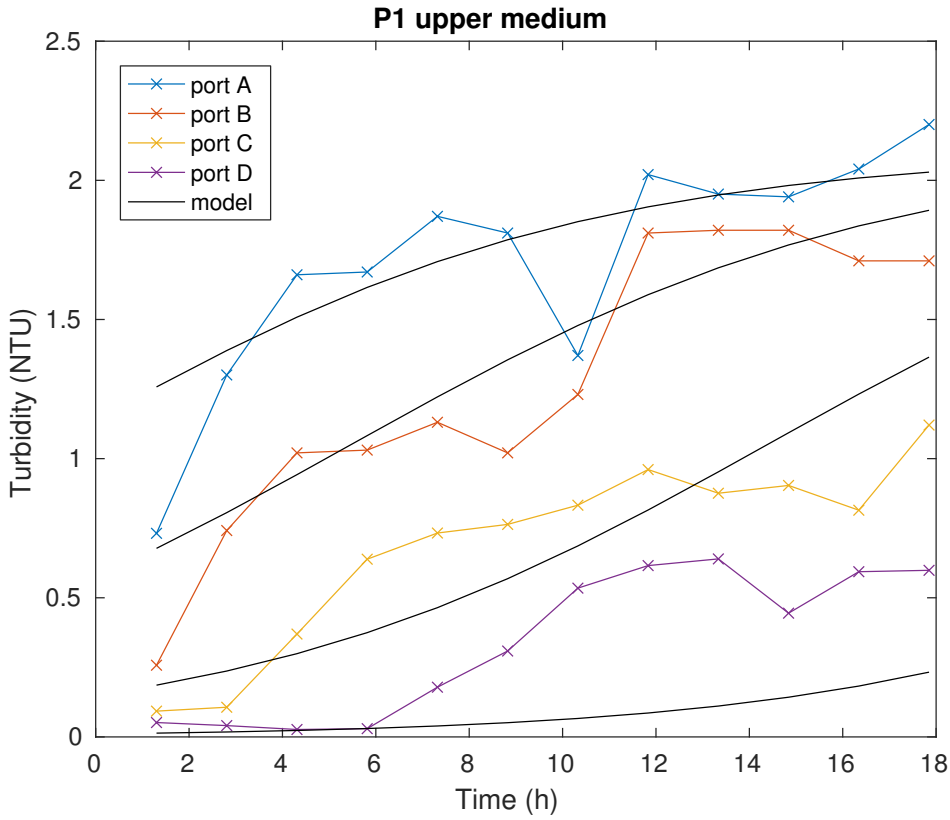

Figure 3.3: Plot of the solution generated by a first-order polynomial in the upper medium considering attachment only. The measured turbidity was also plotted.

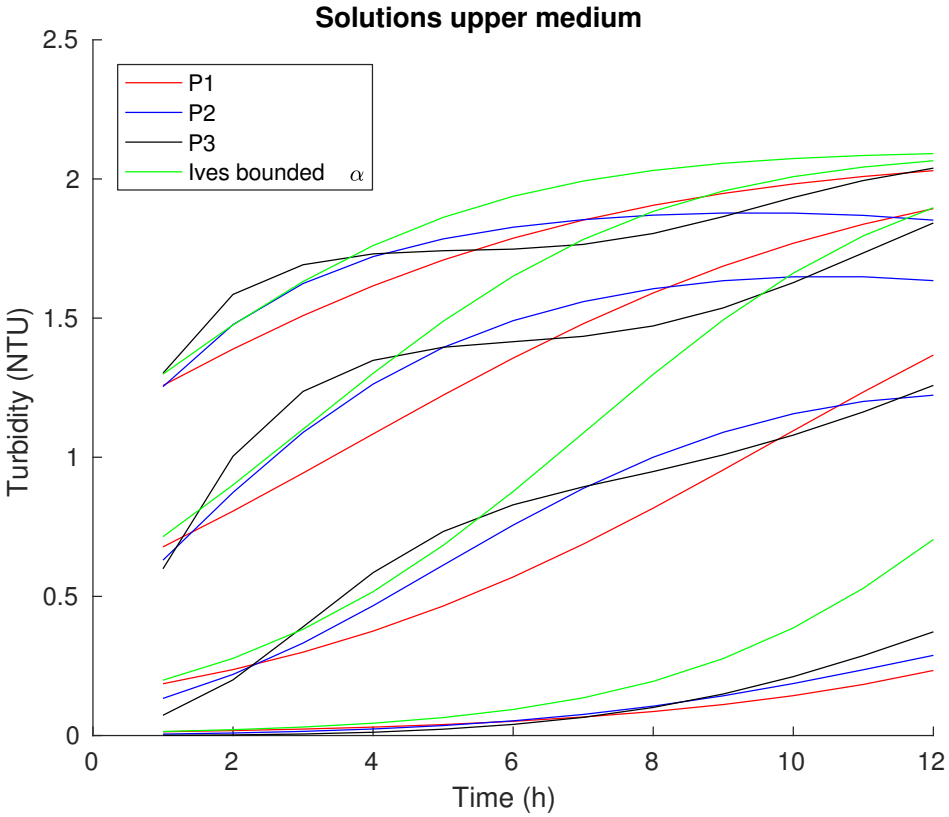

Figure 3.4: The spread of the four most optimal solutions for the upper medium considering attachment only.

3.1.2 Lower medium

From Figure 3.3 and Figure 3.4 it is evident that the model for the upper medium does not match the turbidity observed in port D very well. Looking at Figure 3.5 we see that there is no good optimum for a first-order polynomial in the lower medium when the boundary conditions are set as the output from the upper media. Further experimentations with higher order polynomials led to convergence towards different optimums or just abortion due to low gradients. This could indicate that the problem is ill-posed when the two media are solved separately.

Thus the boundary condition for the lower medium was instead taken as a spline of the turbidity observed in port D, as explained in section 2.6. For the lower medium a first-order polynomial (equation (1.9)), a second-order polynomial (equation (1.10)), a third-order polynomial (equation (1.11)), Ives filtration function with bounded α (equation (1.5)) and Ives filtration function with unbounded α (equation (1.5)) were considered. The optimal filtration functions are shown in Figure 3.6. The weighted relative root mean square, as defined by equation (2.42) and the relative root mean square, as defined by equation (2.43) for the optimal filtration functions was printed in Table 3.3. The weighted relative root mean square, as defined by equation (2.42), for the first-order polynomial for different choices of parameters was printed in Figure 3.7.

From Table 3.3 we can see that the two Ives filtration functions and the third-order polynomial have approximately the same weighted error. Looking at Figure 3.6 we see that Ives filtration functions seems to have a similar shape as the third-order polynomial. This suggests that we can replace Ives filtration function with a third-order polynomial, reducing the number of parameters from 7 to 4. Furthermore, the best fit filtration functions in the lower medium are low for $\sigma_{\text{turb}} = 0$, then increasing with σ_{turb} and then decreasing. This fit very well with the shape one would expect for a typical filter cycle with a ripening period. However, for large values of σ_{turb} the third-order polynomial starts to rise again. Physically this means that very large values of σ_{turb} increases the filter efficiency. This is not supported by observations from filtration theory. By looking at Figure 3.8 we can observe that port E, F and G goes through a ripening, working and breakthrough stage. Since

Filtration function	Weighted RRMSE	RRMSE
P1	0.4007	0.2165
P2	0.3727	0.2309
P3	0.3278	0.2012
Ives	0.3288	0.2072
Ives unbounded α	0.3200	0.1879

Table 3.3: Weighted RRMSE and RRMSE for the optimal filtration functions in the lower medium considering attachment only.

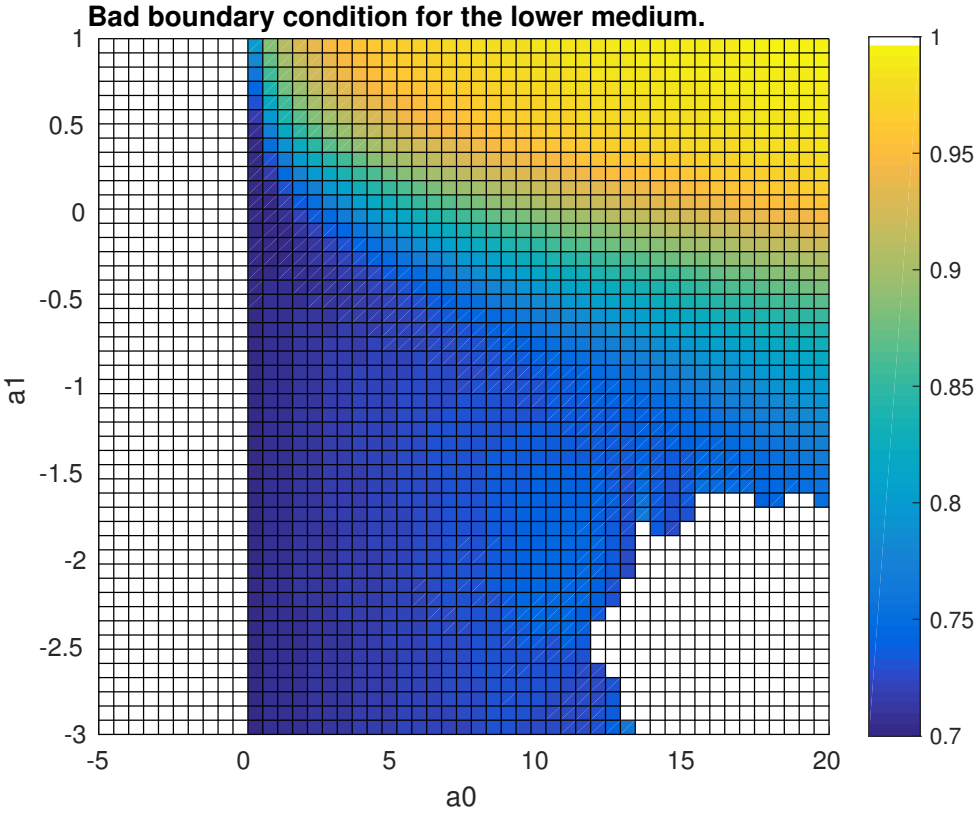

Figure 3.5: Plot of the weighted RRMS for different choices of parameters for the first-order polynomial in the lower medium considering attachment only. Boundary conditions is set as the solution at the end of the upper medium generated by a first-order polynomial. Dark blue colors represents parameters that give a good fit, yellow color represents parameters that give a bad fit. White cells represents parameters that gave large values or NaN values.

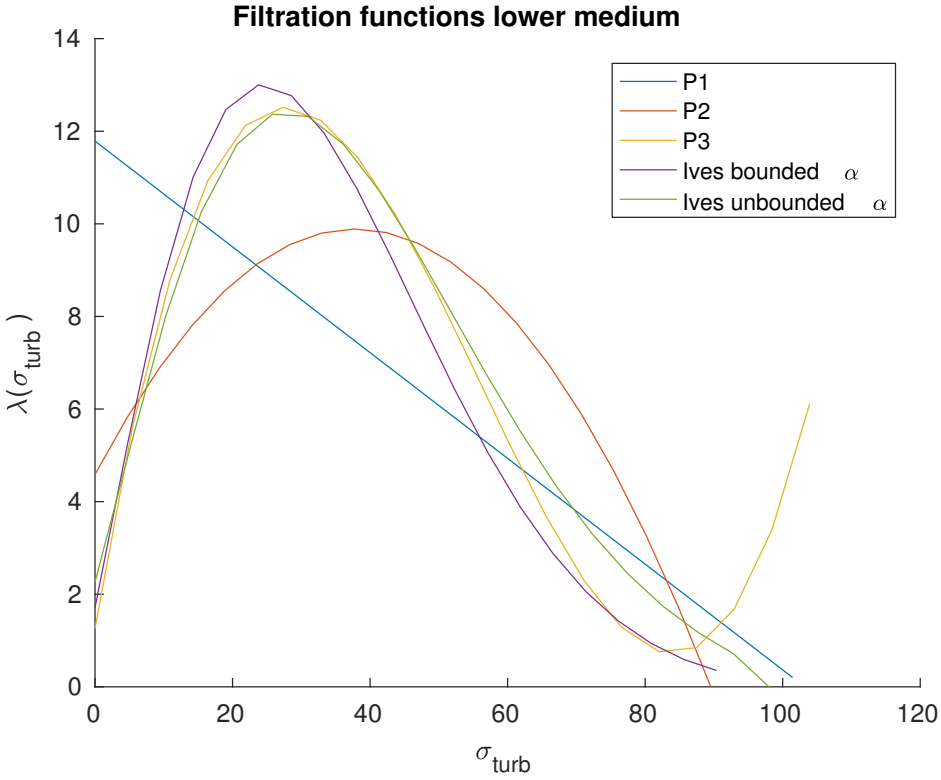

Figure 3.6: Optimal filtration functions for the lower medium considering attachment only. The upper and lower range is set by the largest and smallest σ_{turb} present in the solution.

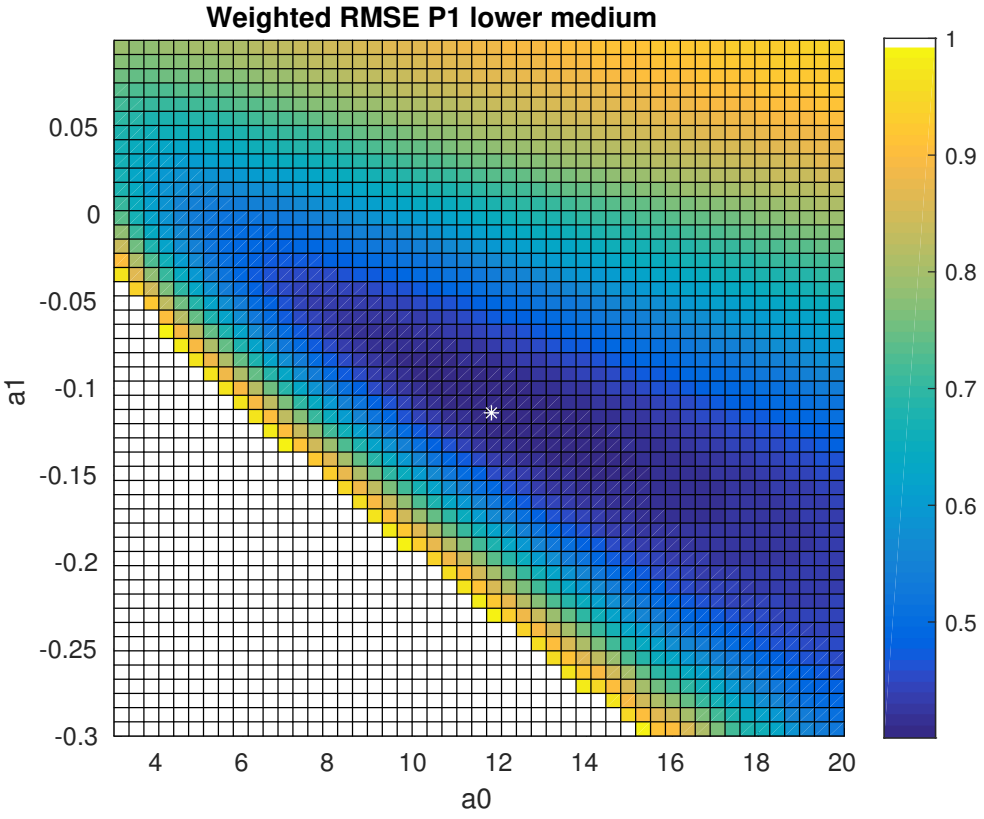

Figure 3.7: Plot of the weighted RRMS for different choices of parameters for the first-order polynomial lower medium considering attachment only. Dark blue colors represents parameters that give a good fit, yellow color represents parameters that give a bad fit. White cells represents parameters that gave large errors or NaN values. The white $*$ is the optimum found by the inverse solver.

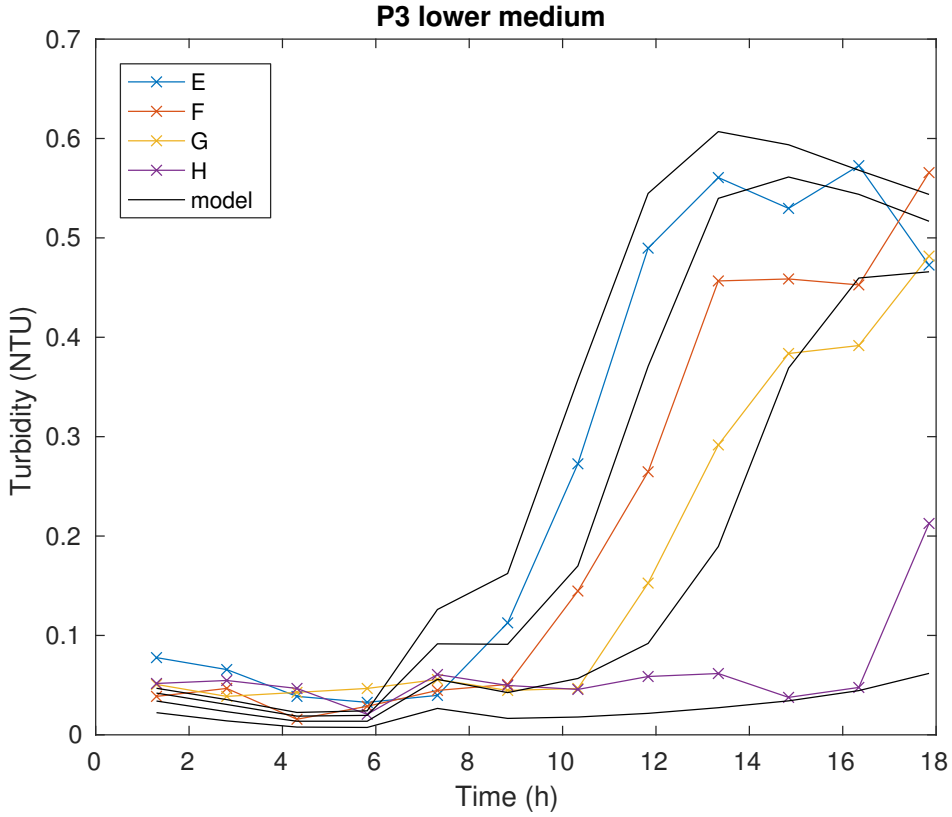

Figure 3.8: Solution generated by a third-order polynomial in the lower medium considering attachment only. The measured turbidity was also plotted.

all stages of the filtration cycle are to some extent captured by the observations, we should expect $\lambda(\sigma_{\text{turb}})$ to reflect this by displaying a rising trend before decreasing again. This could explain the observed qualitative shape of the best-fit filtration functions.

Looking at Figure 3.7 we can observe that the optimum found by the inverse solver is flatter than the optimum found in the upper medium, see Figure 3.2. This indicates that there are more first-order polynomials that could explain the data for the lower medium than for the upper medium and that the answers found in this medium is more uncertain. This is supported by the error printed Table 3.3 where it is suggested a the first-order polynomial is a less good model for this filter. The best fit $\lambda(\sigma_{\text{turb}})$ for the third-order polynomial was used to generate a solution for the lower medium. The solution was printed in Figure 3.8.

Different choices of initial values for the parameters was tested for Ives filtration function in the lower medium. This led to convergence towards different optima or

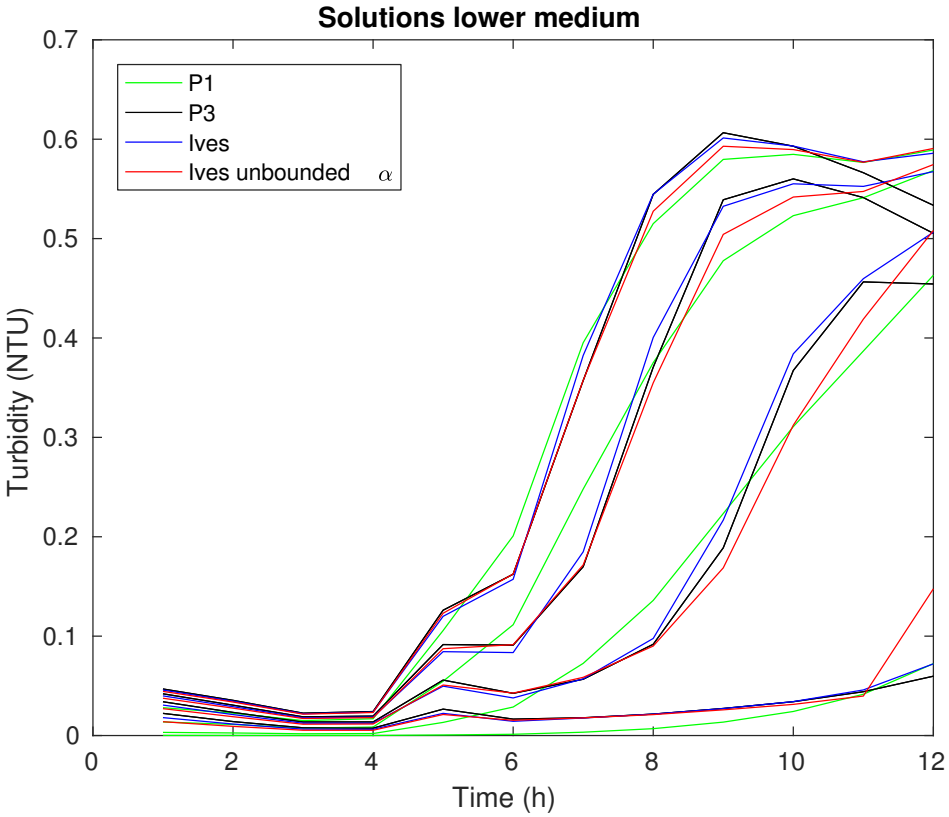

Figure 3.9: The spread of the four most optimal solutions for the lower medium considering attachment only.

	a_0	a_1	a_2	a_3			
P1	11.786	-0.114					
P2	4.588	0.280	-0.004				
P3	1.258	0.915	-0.022	1.313e-04			
	λ_0	β	n_1	n_2	n_3	α	σ_{ult}
Ives	1.709	39.306	1.596	6.406	0.151	311.783	0.422
Ives_α	2.263	29.864	1.967	9.510	0.279	466.729	0.210

Table 3.4: The parameters for the best filtration functions in the lower medium considering attachment only. Ives_α denotes Ives filtration function with unbounded α.

just abortion due to low gradients. There were no such errors for the polynomials. This could indicate that the problem is ill-posed for the Ives filtration function, probably because it has too many parameters.

The parameters for for the best fit filtration functions in the lower medium are shown in Table 3.4.

3.2 Attachment and detachment

For the model considering attachment and detachment the forward Euler scheme described by equation (2.25) and equation (2.26) was applied. Equation (1.6) allowing attachment and detachment was applied with two different filtration functions $\lambda(\sigma_{\text{turb}})$ (for the attachment part) for the upper and the lower medium.

3.2.1 The upper medium

For the upper medium a first-order polynomial (equation (1.9)) and a second-order polynomial (equation (1.10)) was considered for $\lambda(\sigma_{\text{turb}})$. Detachment was described by the affine function $b_1\sigma_{\text{turb}}$, as in equation (1.6). The best fit filtration functions are shown in Figure 3.10. The weighted relative root mean square, as defined by equation (2.42) and the relative root mean square, as defined by equation (2.43) for the best fit $\lambda(\sigma_{\text{turb}})$ was printed in Table 3.5.

Filtration function $\lambda(\sigma)$	**Weighted RRMSE**	**RRMSE**
First-order polynomial	0.1762	0.1456
Second-order polynomial	0.1677	0.1367

Table 3.5: Weighted RRMS and RRMS for the optimal filtration functions in the upper medium considering attachment and detachment.

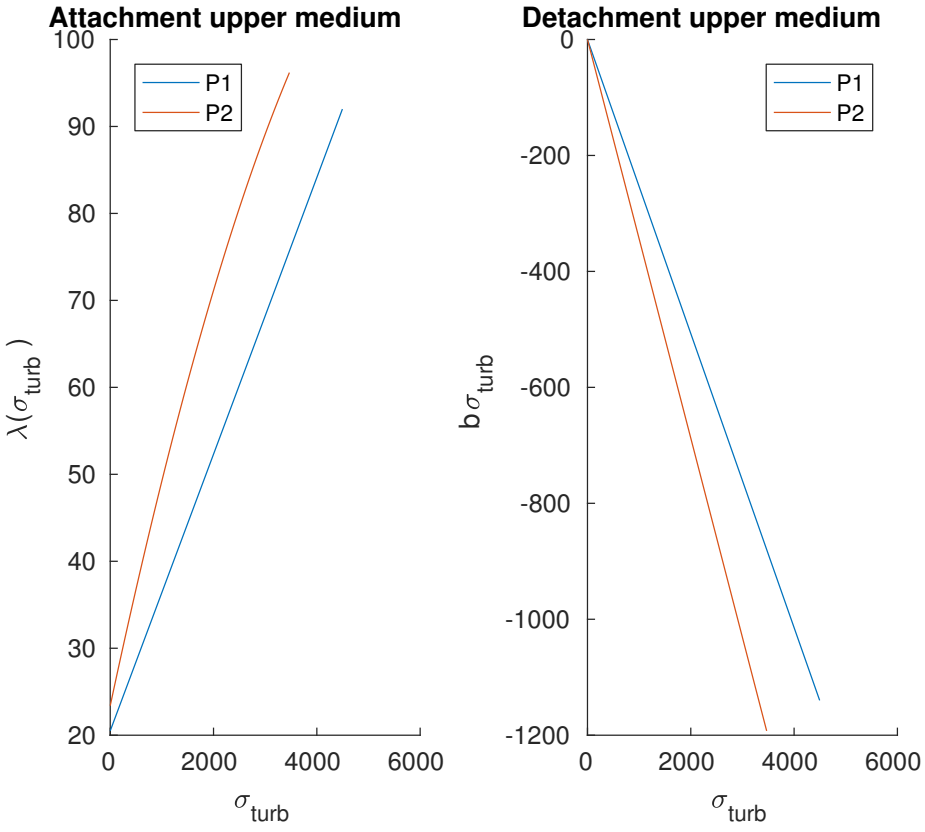

Figure 3.10: Optimal filtration functions for the upper medium considering attachment and detachment. The upper and lower range is set by the largest and smallest σ_{turb} present in the solution.

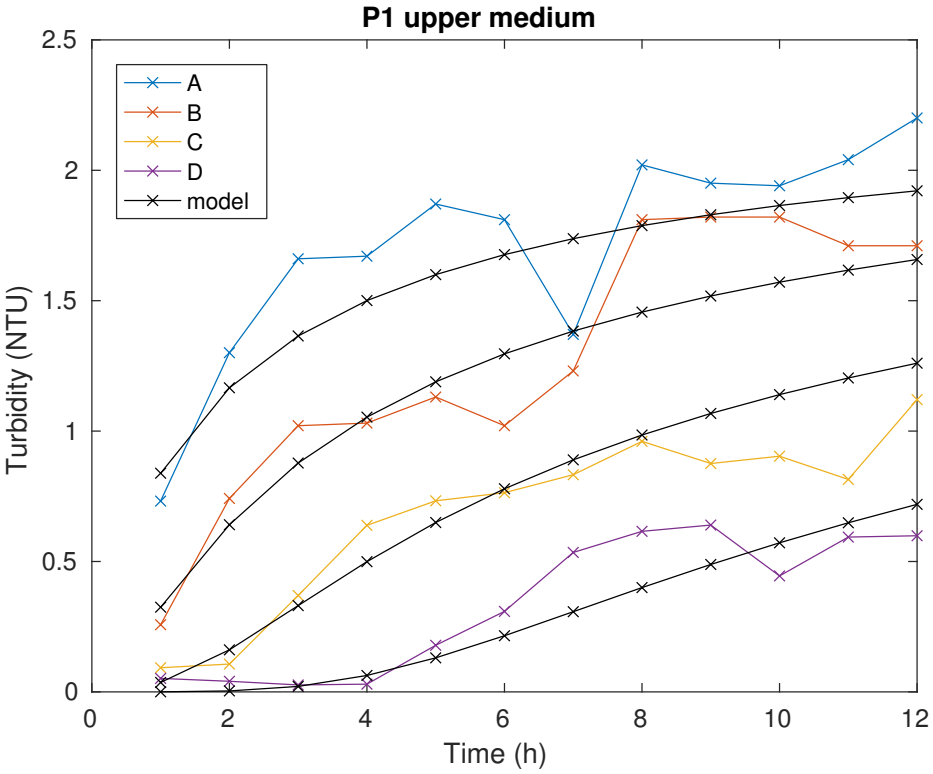

Figure 3.11: Solution generated by a linear attachment function and a linear detachment function in the upper medium. The measured turbidity was also plotted.

From Table 3.5 we see that the relative error for the first-order polynomial has almost the same relative error as the second-order polynomial. Figure 3.10 indicates that they qualitatively have the same shape, low in the beginning, and then rising. Comparing the weighted error we get when detachment is introduced with the weighted error when only attachment is considered, we see that the model allowing detachment gives a much better fit. A solution generated by the first order polynomial along with its corresponding linear detachment function was printed in Figure 3.11. In this Figure we see that the model gives a rather good description of the turbidity observed in port D.

The parameters for for the best fit filtration functions in the upper medium are shown in Table 3.6.

	b_1	a_0	a_1	a_2
P1	-0.2536	20.4999	0.0159	
P2	-0.3438	23.3927	0.0278	-1.9662e-06

Table 3.6: The parameters for the best fit first-order polynomial and the second-order polynomial in the upper medium with detachment.

3.2.2 Lower medium

For the lower medium a first-order polynomial (equation (1.9)) and a second-order polynomial (equation (1.10)) was considered for $\lambda(\sigma_{\text{turb}})$. Detachment was described by the affine function $b_1\sigma_{\text{turb}}$, as in equation (1.6). The best fit filtration functions are shown in Figure 3.12. The weighted relative root mean square, as defined by equation (2.42) and the relative root mean square, as defined by equation (2.43) for the best fit $\lambda(\sigma_{\text{turb}})$ was printed in Table 3.7.

From Table 3.7 we see that the relative error for the first-order polynomial has almost the same relative error as the second-order polynomial. Figure 3.12 indicates that they qualitatively have the same shape, low in the beginning and then rising. Comparing the weighted error when detachment is introduced with the weighted error when only attachment is considered we see that the model that allows detachment only gives a slightly better fit. This could indicate that detachment do not play a role in this medium. A solution generated by the first-order polynomial along with its linear detachment function was printed in Figure 3.13.

The parameters for for the best fit filtration functions in the lower medium are shown in Table 3.8.

Filtration function $\lambda(\sigma)$	**WeightedRMSE**	**RMSE**
First-order polynomial	0.3150	0.1907
Second-order polynomial	0.3084	0.1692

Table 3.7: Weighted RRMS and RRMS for the optimal filtration functions in the lower medium considering attachment and detachment.

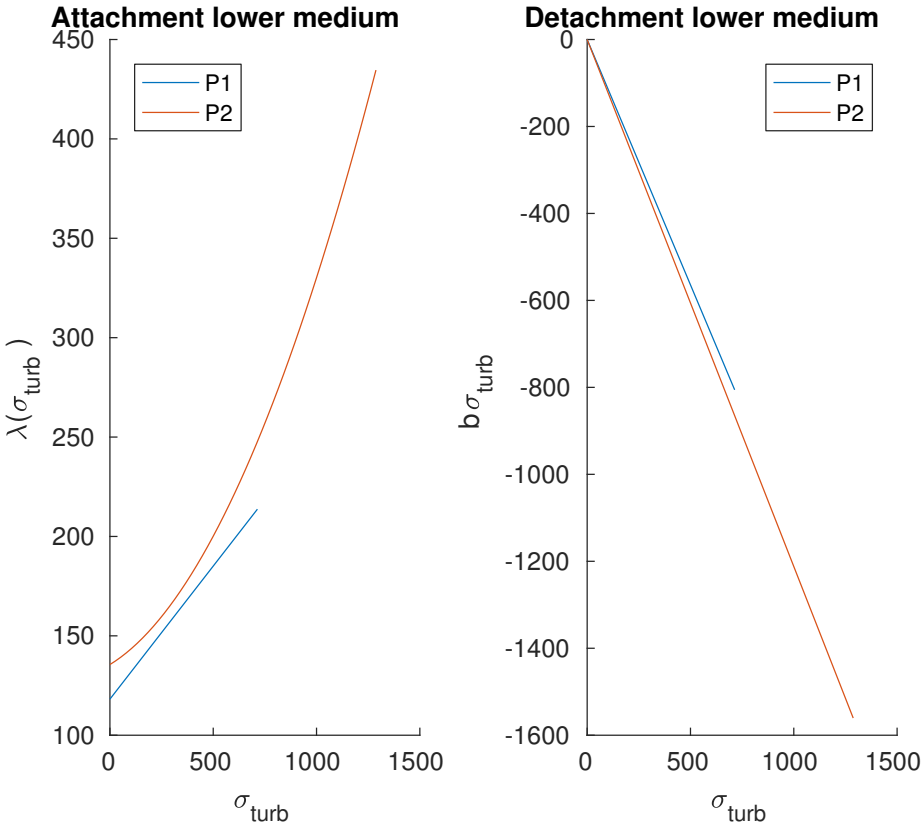

Figure 3.12: Optimal filtration functions for the lower medium considering attachment and detachment. The upper and lower range is set by the largest and smallest σ_{turb} present in the solution.

	b_1	a_0	a_1	a_2
P1	-1.1286	118.1499	0.1339	
P2	-1.2120	135.5478	0.0637	1.3092e-04

Table 3.8: The parameters for the best fit first-order polynomial and the second-order polynomial in the lower medium with detachment.

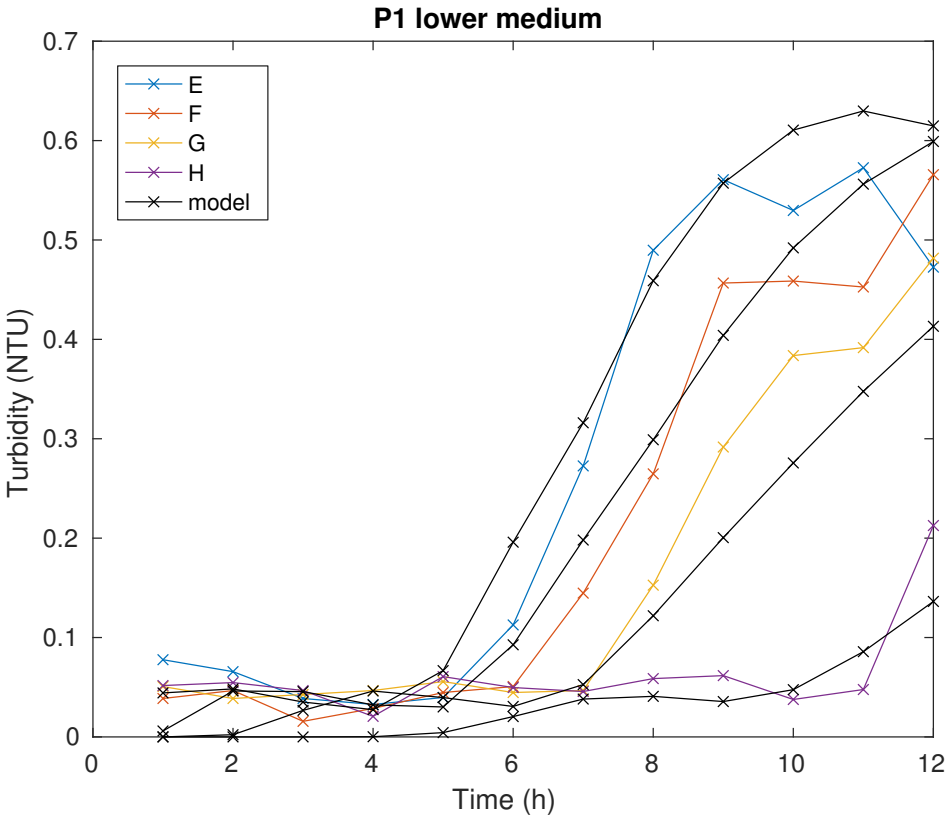

Figure 3.13: Solution generated by a linear attachment function and a linear detachment function in the lower medium. The measured turbidity was also plotted.

3.3 General discussion

3.3.1 Uncertainties in measurements

None of the models presented above gave a perfect fit to the measured data. Our model should produce smooth lines, but looking at the recordings in Figure 1.3 we see that turbidity does not follow completely smooth lines. Thus there are uncertainties in the measurements and in the model. One uncertainty in the measurements is that the turbidity from the auto-sampler was measured after the whole filter run was complete. Thus residual-coagulant could have affected the samples. Other uncertainties in the measurements include uncertainties in the apparatus measuring the turbidity. It must also be noted that although the observations have a high resolution they are only based on one filtration cycle.

3.3.2 Uncertainties in turbidity-particle relation

In our model we have assumed that the turbidity is proportional to the volume of particles. This is true for unfiltered water where the distribution of particle sizes can reasonably be assumed not to be changing, see section 2.5. However, from previous studies we know that the breakthrough front propagates at different speed for different particle sizes, see section 1.3.2. Thus the assumption that turbidity is proportional to particle-volume is good for the early stages of the filtration and increasingly worse with time. Further, larger particles will deposit more easily than smaller particles, maing them deposit in the upper parts of the filter medium. Thus the assumption that turbidity is proportional to particle-volume is good for the upper parts of the filter medium and increasingly worse with depth.

3.3.3 Uncertainties in porosity

Another assumption is that the two filter media are completely separated; this is not true as the two media will intermix a little in an interface zones between them. Within one filter medium there will also be some sorting of grain-sizes, with the finest grains on the top. This happens due to backwashing. As a result we do not have two perfect homogeneous layers and the porosity is a function of filter depth. In the models we have also assumed that the porosity is constant throughout the filter cycle. We can better understand the effects of porosity by looking at the characteristic lines of equation (1.1) defined by equation (C.5) and equation (C.6). Here ϵ determines the slope of the characteristic line and is a function of time and space. According to equation (2.5), as the particles deposit in the filter medium the porosity decreases. Thus it follows that the slope of the characteristic line also decreases. This indicates that the characteristic lines of equation (1.1) becomes

similar to the characteristic lines of equation (2.23). However, this needs more investigations.

3.3.4 Uncertainties in the boundary conditions

Finding a good spline for the boundary condition for the lower medium was not easy. As can bee seen in Figure 2.3, the turbidity recorded in port D is actually lower than the turbidity recorded in port E. This created large relative errors in the first 6 hours of the filtration cycle. Attempts to fit a smoothed spline did not give a much better fit. In the end a simple quadratic spline was used.

3.3.5 Uncertainties in the mathematical schemes

The mathematical method used to solve the system with only attachment is solving a system of ordinary differential equations. This is a stable and fast method that has been applied in other studies as well. For Ives filtration function the optimum seemed to be very flat as the optimization routine gave different results and aborted due to low gradients. For the polynomials there were no problems with low gradients and there seems to be somewhat well-defined optima for the upper and the lower medium, see Figure 3.2 and Figure 3.7. The mathematical method used to solve the system when detachment is included is not so fast and reliable and the optima have not been studied as closely as with the model considering only attachment. However, the method gave a better fit to the measured data for the upper medium, indicating that effects from detachment are important. There was no abortion due to low gradients. A more reliable method for solving the forward problem was derived but not implemented.

3.3.6 Whether to include detachment

In the upper medium the models fit better with the observations if particles are allowed to detach. However, even if detachment is included in the model we do not get the flattening tendency that the data shows towards the end of the filtration runs, see Figure 1.3.

3.3.7 Retained particles

A plot of the retained turbidity considering only attachment and a third-order filtration function at the end of the filtration cycle are shown in Figure 3.14. A plot of the retained turbidity considering a affine attachment function and a linear detachment function at the end of the filtration cycle are shown in Figure 3.15.

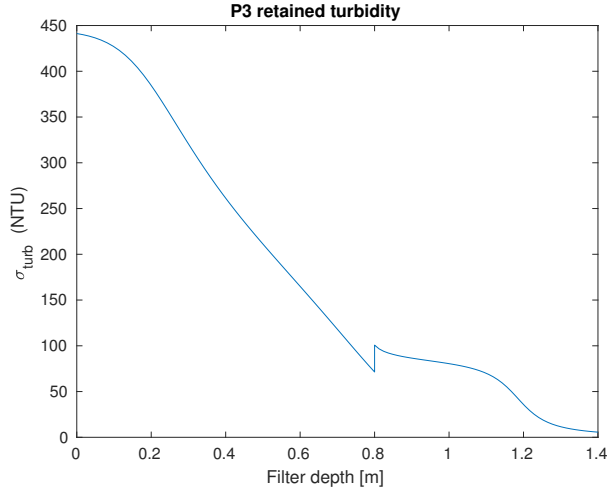

Figure 3.14: The retained turbidity at $T = 18$ for different filter depths considering attachment only. Boundary conditions are set as spline of observations in port D.

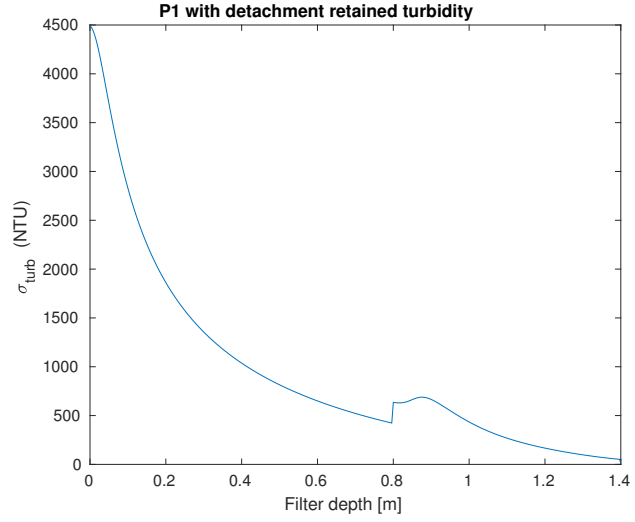

Figure 3.15: The retained turbidity at $T = 18$ for different filter depths considering attachment and detachment. Boundary conditions are set as spline of observations in port D.

The two solutions seem to give quite different results in the upper and the lower medium. The sharp edge at z=0.8 in Figure 3.15 comes from a small error in the implementation of the numerical scheme, where σ in the last row of the grid was not taken into account. The two methods seem to give very different solutions in the upper medium and not that much difference in the lower medium.

Chapter 4

Conclusions

In this thesis we wanted to find filtration functions that made the model fit to measured data. We have developed two different methods that solve the forward problem given a set of parameters, the forward Euler scheme and the method that solves a system of ODEs. These methods seem to give the same results for a fine spaced grid for models that only allow attachment. The forward Euler scheme was extended to allow particles to detach.

When only attachment was considered the third-order polynomial gave the best result in the upper medium. However, the third order polynomial did not perform much better than a first-order polynomial. For the lower medium the third-order polynomial gave almost as good fit as Ives filtration function. Here the first-order polynomial gave poor results. When detachment was introduced the model for the upper medium gave a much better fit, even if the model had very few parameters. The retained turbidity at the end of the filter cycle was different between the model that allowed detachment and the model that allowed only attachment. This happened even in the lower medium, where the errors was quite similar. However, in order to conclude anything about particle removal more filtration runs are needed.

In this thesis we also wanted to find a more transparent derivation of Herzig's method for solving the system of ODEs. It turns out that the concept of "corrected time" can be thought of as following a particle along its streamlines. It was also shown in Appendix C that the general derivation of equation (2.36) does not need to assume constant porosity. Although there were no time to implement these findings in the solution algorithms, they can be used in further investigations. Further investigations should study how changing porosity affects the filtration model.

It is recommended that further investigations focus on implementing a faster solution method that allows detachment. This could be for instance the method of lines or the method of characteristics method derived in Appendix D. It is also sug-

gested that further investigations try to solve the two media simultaneous, if there is a great need for a solution that is continuous on the interface between the filter media.

As the ripening stage in the upper medium was over when the first measurement was done, it is recommended that further experiments use a longer filter in the upper part. From the simulations it seems that using a spline of the turbidity recorded inside the media as a boundary condition to the forward problem gives meaningful results. However, this might not be very representative for a real DWTP where the filter medium is not so deep. A better suggestion might be to do more frequent sampling in the early stages of the filtration cycle.

References

Adin, A. and Rebhun, M. (1974). High-Rate Contact Flocculation—Filtration with Cationic Polyelectrolytes. *Journal - American Water Works Association* **66** (2), pp. 109–117. URL: http://www.jstor.org/stable/41266974.

Adin, A. and Rebhun, M. (1977). A Model to Predict Concentration and Head-Loss Profiles in Filtration. *Journal - American Water Works Association* **69** (8), pp. 444–453. URL: http://www.jstor.org/stable/41269018.

Adin, A. and Rajagopalan, R. (1989). Breakthrough Curves in Granular Media Filtration. *Journal of Environmental Engineering* **115** (4), pp. 785–798. DOI: 10.1061/(ASCE)0733-9372(1989)115:4(785).

Alvarez, A. C. (2005). Inverse Problems for Deep Bed Filtration in Porous Media. PhD thesis. Instituto Nacional de Matemática Pura e Aplicada, Rio de Janeiro, Brasil, pp. 13–14. URL: http://preprint.impa.br/visualizar?id=6841.

Amirtharajah, A. and Mills, K. M. (1982). Rapid-Mix Design for Mechanisms of Alum Coagulation. *Journal - American Water Works Association* **74** (4), pp. 210–216. URL: http://www.jstor.org/stable/41271001.

Bache, D. H. and Gregory, R. (2010). Flocs and Separation Processes in Drinking Water Treatment: A Review. *Journal of Water Supply: Research and Technology—AQUA* **59** (1), pp. 16–30. DOI: 10.2166/aqua.2010.028.

Bai, R. and Tien, C. (2000). Effect of Deposition in Deep-Bed Filtration: Determination and Search of Rate Parameters. *Journal of Colloid and Interface Science* **231** (2), pp. 299–311. DOI: 10.1006/jcis.2000.7130.

Boorman, G. A., Dellarco, V., Dunnick, J. K., Chapin, R. E., Hunter, S., Hauchman, F., Gardner, H., Cox, M., and Sills, R. C. (1999). Drinking Water Disinfection Byproducts: Review and Approach to Toxicity Evaluation. *Environmental Health Perspectives* **107** (Suppl. 1), pp. 207–217. URL: http://www.ncbi.nlm.nih.gov/pubmed/10229719.

Clark, S. C., Lawler, D. F., and Cushing, R. S. (1992). Contact Filtration: Particle Size and Ripening. *Journal - American Water Works Association* **84** (12), pp. 61–71. URL: http://www.jstor.org/stable/41293944.

Crozes, G., White, P., and Marshall, M. (1995). Enhanced Coagulation: its effect on NOM removal and chemical costs. *Journal - American Water Works Association* **87** (1), pp. 78–89. URL: http://www.jstor.org/stable/41295154?seq=1%5C#page%5C_scan%5C_tab%5C_contents.

Edzwald, J. K. and Tobiason, J. E. (1999). Enhanced Coagulation: US Requirements and a Broader View. *Water Science & Technology* **40** (9), pp. 63–70. DOI: 10.1016/S0273-1223(99)00641-1.

Eikebrokk, B. (2012). *Veiledning for drift av koaguleringsanlegg*. Tech. rep. 188/2012, p. 155. URL: http://goo.gl/iA6T54.

Folkehelseinstituttet (2016). *Vannrapport 127: Vannforsyning og helse. Veiledning i drikkevannshygiene*. Ed. by E. Andersen. Folkehelseinstituttet. Chap. 4, pp. 63–68. URL: https://www.fhi.no/publ/2016/vannrapport-127/.

Havelaar, A. H., De Hollander, A. E. M., Teunis, P. F. M., Evers, E. G., Van Kranen, H. J., Versteegh, J. F. M., Van Koten, J. E. M., and Slob, W. (2000). Balancing the Risks and Benefits of Drinking Water Disinfection: Disability Adjusted Life-Years on the Scale. *Environmental Health Perspectives* **108** (4), pp. 315–321. DOI: 10.1289/ehp.00108315.

Herzig, J. P., Leclerc, D. M., and Le Goff, P. (1970). Flow of Suspensions Through Porous Media—Application to Deep Filtration. *Industrial & Engineering Chemistry* **62** (5), pp. 8–35. DOI: 10.1021/ie50725a003.

Hijnen, W. A. M. and Medema, G. J. (2010). *Elimination of Microorganisms by Water Treatment Processes*. IWA Publishing, p. 160. DOI: 10.2166/9781780401584.

Horner, R. M. W., Jarvis, R. J., and Mackie, R. I. (1986). Deep Bed Filtration: A New Look at the Basic Equations. *Water Research* **20** (2), pp. 215–220. DOI: 10.1016/0043-1354(86)90011-4.

Ives, K. J. (1969). Modern Theory of Filtration. Special Subject No. 7. In: *International Water Supply Congress and Exhibition, Vienna 1969*. London: International Water Supply Association.

Iwasaki, T. (1937). Some Notes on Sand Filtration. *Journal - American Water Works Association* **29** (10), pp. 1591–1602. URL: http://www.jstor.org/stable/41231759.

Jegatheesan, V. and Vigneswaran, S. (2005). Deep Bed Filtration: Mathematical Models and Observations. *Critical Reviews in Environmental Science and Technology* **35** (6), pp. 515–569. DOI: 10.1080/10643380500326432.

Kim, J. K. and Lawler, D. F. (2006). Particle Detachment During Hydraulic Shock Loads in Granular Media Filtration. *Water Science & Technology* **53** (7), pp. 177–184. DOI: 10.2166/wst.2006.222.

LeVeque, R. J. (1992). *Numerical Methods for Conservation Laws*. 2nd ed. URL: http://www.springer.com/in/book/9783764327231.

Logan, J. D. (2001). *Transport Modeling in Hydrogeochemical Systems*. Vol. 15. Interdisciplinary Applied Mathematics. New York, NY: Springer New York, p. 225. DOI: 10.1007/978-1-4757-3518-5.

Mattilsynet (2011). *Veiledning til Drikkevannsforskriften*. URL: http://goo.gl/4QPw4B.

Mints, D. M. (1966). Modern Theory of Filtration. Special Subject No. 10. In: *International Water Supply Congress, Barcelona 1966*. London: International Water Supply Association.

Moran, M. C., Moran, D. C., Cushing, R. S., and Lawler, D. F. (1993). Particle Behavior in Deep-Bed Filtration: Part 2—Particle Detachment. *Journal - American Water Works Association* **85** (12), pp. 82–93. URL: http://www.jstor.org/stable/41294462.

Nilsen, V. (2016). Quantitative Microbial Risk Assessment for Drinking Water: Dose-Response Theory and Virus Filtration Dynamics. PhD thesis. URL: http://hdl.handle.net/11250/2433906.

O'Melia, C. R. (1985). Particles, Pretreatment, and Performance in Water Filtration. *Journal of Environmental Engineering* **111** (6), pp. 874–890. DOI: 10.1061/(ASCE)0733-9372(1985)111:6(874).

Petterson, S. R. and Ashbolt, N. J. (2016). QMRA and Water Safety Management: Review of Application in Drinking Water Systems. *Journal of Water and Health* **14** (4), pp. 571–589. DOI: 10.2166/wh.2016.262.

Richard E. Ewing, H. W. (2001). A summary of numerical methods for time-dependent advection-dominated partial differential equations. *Journal of computational and applied mathematics* **128** (1 - 2), pp. 423–445. URL: http://www.sciencedirect.com/science/article/pii/S0377042700005227.

Tien, C. and Ramaro, B. V. (2007). *Granular Filtration of Aerosols and Hydrosols*. 2nd ed. Butterworth-Heinemann, p. 512. URL: http://www.sciencedirect.com/science/book/9781856174589.

Appendices

Appendix A

Deriving the conservation law

Let Ω be an arbitrary subinterval of the interval $[0, Z]$, where Z is the length of our porous filter media bed [L]. We start by dividing Ω into N subintervals, $\Omega = [z_1, z_N]$. The volume of the particles in each of these subintervals is approximately given as

$$\Delta S_n(t) \approx \epsilon(z_n, t)c(z_n, t)A(z_n, t)\Delta z_n.$$

Where $\epsilon(z_n, t)$ is the porosity given as volume water per volume filter [L^3/L^3], $c(z_n, t)$ is the volume concentration of particles in the water phase [L^3/L^3], $A(z_n, t)$ is the cross sectional area [L^2] and $\Delta\ z_n$ is the height of the porous media element [L]. Then the total volume of the particles stored in our filter can be found by summing all the contributions from the subintervals

$$S(t) \approx \sum_{n=1}^{N} \epsilon(z_n, t)c(z_n, t)A(z_n, t)\Delta z_n.$$

Taking the Riemann-sum as $\Delta z \to 0$ we get

$$S(t) = \int_{z_1}^{z_N} \epsilon(z, t)c(z, t)A(z, t)dz.$$

$S(t)$ is only changing if particles are transported into Ω or if particles are attached or detached inside Ω. Hence

$$\frac{\partial S}{\partial t} = F + P, \tag{A.1}$$

where F denotes the particles transported across the boundary $\partial\Omega$ into Ω and P denotes the attachement/detachment inside Ω. First we consider the transport term F. Neglecting effects from diffusion and dispersion, particles are only transported into and out of our system through the cross sections z_1 and z_N by the free water masses

$$F(t) = \left(c(z_1,t)u(z_1,t)A(z_1,t) - c(z_N,t)u(z_N,t)A(z_N,t)\right).$$

Where $c(z_n,t)$ is the volume of particles per volume water $[\mathrm{L}^3/\mathrm{L}^3]$ and $u(z_n,t)$ is the Darcy velocity of the fluid [L/T]. By the fundamental theorem of calculus

$$F(t) = -\int_{z_1}^{z_N} \frac{\partial}{\partial z}\left[c(z,t)u(z,t)A(z,t)\right] dz. \tag{A.2}$$

The last term P will in our case denote the rate at which particles attach and detach inside Ω. The volume of the particles in each of the subintervals $\Omega = [z_1, z_N]$ is approximately given as

$$\Delta W_n(t) \approx \sigma(z_n,t)A(z_n,t)\Delta z_n.$$

Where σ is the retention, that is, volume of deposited particles per volume filter $[\mathrm{L}^3/\mathrm{L}^3]$. Now the total volume of the particles stored in our filter can be found by summing all the contributions from the subintervals

$$W(t) \approx \sum_{n=1}^{N} \sigma(z_n,t)A(z_n,t)\Delta z_n.$$

Taking the Riemann-sum as $\Delta z \to 0$ we get

$$W(t) = \int_{z_1}^{z_N} \sigma(z,t)A(z,t)dz.$$

Letting P be the negative rate of change of $W(t)$ we can define a general filtration function

$$P = -\frac{\partial W}{\partial t} = -\frac{\partial}{\partial t}\int_{z_1}^{z_N} \sigma(z,t)A(z,t)dz. \tag{A.3}$$

Combining (A.1), (A.2) and (A.3) we get

$$\frac{\partial}{\partial t}\int_{z_1}^{z_N} \epsilon(z,t)c(z,t)A(z,t)dz = -\int_{z_1}^{z_N} \frac{\partial}{\partial z}\left[c(z,t)u(z,t)A(z,t)\right] dz - \frac{\partial}{\partial t}\int_{z_1}^{z_N} \sigma(z,t)A(z,t)dz,$$

Assuming $\epsilon(z,t)$, $c(z,t)$, $\sigma(z,t)$ and $A(z,t)$ are continuous differentiable in Ω we can interchange derivation and integration

$$\int_{z_1}^{z_N} \frac{\partial}{\partial t} \left[\epsilon(z,t)c(z,t)A(z,t)dz\right] = -\int_{z_1}^{z_N} \frac{\partial}{\partial z} \left[c(z,t)u(z,t)A(z,t)\right] dz - \int_{z_1}^{z_N} \frac{\partial}{\partial t} \left[\sigma(z,t)A(z,t)\right] dz.$$

Rearranging and noticing that $A(z,t)$ and $u(z,t)$ were held constant in our experiment

$$\int_{z_1}^{z_N} \frac{\partial}{\partial t} (c\epsilon) + u\frac{\partial c}{\partial z} + \frac{\partial \sigma}{\partial t} dz = 0 \tag{A.4}$$

Equation (A.4) holds for all intervals in Ω. We define $f(z) = \frac{\partial}{\partial t}(c\epsilon) + u\frac{\partial c}{\partial z} - \frac{\partial \sigma}{\partial t}$. Assuming there exists an a in Ω where $f(a) > 0$. The continuity assumption leads to $f(z) > 0$ for $z \in \Omega_a$ where Ω_a is an interval about a. This implies that we have an interval Ω_a where $\int_{\Omega_a} f(z)dz > 0$ which contradicts (A.4). Thus (A.4) is fulfilled if and only if

$$\frac{\partial}{\partial t}(\sigma + \epsilon c) + u\frac{\partial c}{\partial z} = 0.$$

Appendix B

Derivation of the filtration rate

For particles we start with the simplified volume conservation equation given by equation (2.23). For a model considering attachment only Iwasaki (1937) proposed a exponential filtration rate

$$\frac{\partial c}{\partial z} = -\lambda c.$$

Inserting this into equation (2.23)

$$\frac{\partial \sigma}{\partial t} = u\lambda(\sigma)c.$$

For virus we can simplify the volume conservation equation (1.2) by the method of characteristics

$$\frac{\partial \sigma_v}{\partial t} + u\frac{\partial c_v}{\partial z} = 0.$$

We assume that the virus is attached to larger particles. Thus λ for virus is dependent on how many particles that is captured. We get

$$\frac{\partial c_v}{\partial t} = u\lambda(\sigma)c_v.$$

Thus

$$\frac{\partial \sigma_v}{\partial t} = u\lambda(\sigma)c_v.$$

Appendix C

Deriving the ODE system

The following derivation was done by Bjørn Fredrik Nielsen. It aims at deriving equation (2.36) from equation (1.1)

$$\frac{\partial}{\partial t}\left(\sigma + \epsilon c\right) + u\frac{\partial c}{\partial z}. \tag{C.1}$$

Given a filtration rate on the form of equation (2.28) we have that

$$c = \frac{1}{u\lambda(\sigma)}\frac{\partial \sigma}{\partial t}. \tag{C.2}$$

Substituting $F(\sigma) = \frac{1}{\lambda(\sigma)}$ and inserting equation (C.2) into equation (C.1)

$$\frac{\partial}{\partial t}\left(\sigma + \frac{\epsilon}{u}F(\sigma)\frac{\partial \sigma}{\partial t}\right) + \frac{\partial}{\partial z}\left(F(\sigma)\frac{\partial \sigma}{\partial t}\right) = 0.$$

By the product rule and the chain rule

$$\frac{\partial}{\partial t}\left(\sigma + \frac{\epsilon}{u}F(\sigma)\frac{\partial \sigma}{\partial t}\right) + \frac{\partial}{\partial \sigma}\left(F(\sigma)\right)\frac{\partial \sigma}{\partial z}\frac{\partial \sigma}{\partial t} + F(\sigma)\frac{\partial}{\partial z}\left(\frac{\partial \sigma}{\partial t}\right) = 0.$$

Rearranging

$$\frac{\partial}{\partial t}\left(\sigma + \frac{\epsilon}{u}F(\sigma)\frac{\partial \sigma}{\partial t}\right) + \frac{\partial}{\partial \sigma}\left(F(\sigma)\right)\frac{\partial \sigma}{\partial t}\frac{\partial \sigma}{\partial z} + F(\sigma)\frac{\partial}{\partial t}\left(\frac{\partial \sigma}{\partial z}\right) = 0.$$

By the product rule and the chain rule

$$\frac{\partial}{\partial t}\left(\sigma + \frac{\epsilon}{u}F(\sigma)\frac{\partial \sigma}{\partial t}\right) + \frac{\partial}{\partial t}\left(F(\sigma)\right)\frac{\partial \sigma}{\partial z} + F(\sigma)\frac{\partial}{\partial t}\left(\frac{\partial \sigma}{\partial z}\right) = 0.$$

Simplifying

$$\frac{\partial}{\partial t}\left(\sigma + \frac{\epsilon}{u}F(\sigma)\frac{\partial \sigma}{\partial t} + F(\sigma)\frac{\partial \sigma}{\partial z}\right) = 0.$$

Which implies that

$$\sigma + \frac{\epsilon}{u}F(\sigma)\frac{\partial \sigma}{\partial t} + F(\sigma)\frac{\partial \sigma}{\partial z} = g \tag{C.3}$$

Where

$$g = g(z) = \sigma(z,0) + \frac{\epsilon}{u}F(\sigma(z,0))\frac{\partial \sigma}{\partial t}(z,0) + F(\sigma(z,0))\frac{\partial \sigma}{\partial z}(z,0)$$

If we use the initial conditions

$$c(z,0) = \sigma(z,0) = 0 \quad z \geq 0$$

and assume that equation (C.2) also holds for $t = 0$, then

$$\frac{\partial \sigma}{\partial z}(z,0) = 0 \quad z \geq 0,$$
$$\frac{\partial \sigma}{\partial t} = u\lambda(\sigma(z,0))c(z,0) = 0,$$

and hence

$$g(z) = 0, \quad z \geq 0.$$

It thus follows from equation (C.3) that

$$\frac{\partial \sigma}{\partial z} + \frac{\epsilon}{u}\frac{\partial \sigma}{\partial t} = -\lambda(\sigma)\sigma.$$

Applying the method of characteristics

$$\frac{\partial \sigma}{\partial s} = \frac{\partial \sigma}{\partial z}\frac{\partial z}{\partial s} + \frac{\partial \sigma}{\partial t}\frac{\partial t}{\partial s}, \tag{C.4}$$
$$\frac{\partial z}{\partial s} = 1, \tag{C.5}$$
$$\frac{\partial t}{\partial s} = \frac{\epsilon}{u}, \tag{C.6}$$

we find that

$$\frac{\partial \sigma}{\partial s} = -\lambda(\sigma)\sigma.$$

Notice that this will also work for $\epsilon = \epsilon(z,t)$.

Appendix D

Deriving the ODE system with detachment

The following derivation was done by Bjørn Fredrik Nielsen. It aims at deriving a solution method for the volume conservation equation (1.1) with a filtration rate that allows detachment. Given a filtration rate on the form of equation (1.6) we have that

$$c = \frac{1}{u\lambda(\sigma)}\frac{\partial \sigma}{\partial t} - \frac{1}{u\lambda(\sigma)}g(\sigma). \tag{D.1}$$

Substituting $F(\sigma) = \frac{1}{\lambda(\sigma)}$ and $G(\sigma) = \frac{g(\sigma)}{\lambda(\sigma)}$ and inserting equation (D.1) into equation (1.1)

$$\frac{\partial}{\partial t}(\sigma + \epsilon c) + u\frac{\partial}{\partial z}\left(\frac{F(\sigma)}{u}\frac{\partial \sigma}{\partial t} - \frac{G(\sigma)}{u}\right) = 0.$$

By the product rule and the chain rule

$$\frac{\partial}{\partial t}(\sigma + \epsilon c) + \frac{\partial F}{\partial \sigma}\frac{\partial \sigma}{\partial z}\frac{\partial \sigma}{\partial t} + F(\sigma)\frac{\partial}{\partial z}\frac{\partial \sigma}{\partial t} - \frac{\partial G}{\partial \sigma}\frac{\partial \sigma}{\partial z} = 0.$$

Rearranging

$$\frac{\partial}{\partial t}(\sigma + \epsilon c) + \frac{\partial F}{\partial \sigma}\frac{\partial \sigma}{\partial t}\frac{\partial \sigma}{\partial z} + F(\sigma)\frac{\partial}{\partial t}\frac{\partial \sigma}{\partial z} - \frac{\partial G}{\partial \sigma}\frac{\partial \sigma}{\partial z} = 0.$$

By the product rule and the chain rule

$$\frac{\partial}{\partial t}(\sigma + \epsilon c) + \frac{\partial}{\partial t}\left(F(\sigma)\frac{\partial \sigma}{\partial z}\right) - \frac{\partial G}{\partial \sigma}\frac{\partial \sigma}{\partial z} = 0.$$

Integration with respect to t from 0 to $\tilde{t}$

$$\sigma + \epsilon c + F(\sigma) s \frac{\partial \sigma}{\partial z} - \int_0^{\tilde{t}} \frac{\partial G}{\partial \sigma} \frac{\partial \sigma}{\partial z} dt = 0.$$

Inserting equation (D.1)

$$\sigma + \frac{\epsilon}{u} F(\sigma) \frac{\partial \sigma}{\partial t} - \frac{\epsilon}{u} G(\sigma)\ F(\sigma) \frac{\partial \sigma}{\partial z} - \int_0^{\tilde{t}} \frac{\partial G}{\partial \sigma} \frac{\partial \sigma}{\partial z} dt = 0.$$

Hence,

$$\frac{\partial \sigma}{\partial z} + \frac{\partial \sigma}{\partial t} \frac{\epsilon}{u} = -\lambda(\sigma)\sigma + \frac{\epsilon}{u} g(\sigma) - \lambda(\sigma) \int_0^{\tilde{t}} \frac{\partial G}{\partial \sigma} \frac{\partial \sigma}{\partial z} dt$$

Applying the method of characteristics

$$\begin{aligned} \frac{\partial \sigma}{\partial s} = \frac{\partial \sigma}{\partial z} \frac{\partial z}{\partial s} + \frac{\partial \sigma}{\partial t} \frac{\partial t}{\partial s}, \\ \frac{\partial z}{\partial s} = 1, \\ \frac{\partial t}{\partial s} = \frac{\epsilon}{u}. \end{aligned}$$

Then

$$\frac{d\sigma}{ds} = -\lambda(\sigma)\sigma + \frac{\epsilon}{u} g(\sigma) - \lambda(\sigma) \int_0^{\tilde{t}(s)} \frac{\partial G}{\partial \sigma} \frac{\partial \sigma}{\partial z} dt$$

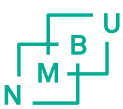

Norges miljø- og biovitenskapelig universitet
Noregs miljø- og biovitskapelege universitet
Norwegian University of Life Sciences

Postboks 5003
NO-1432 Ås
Norway